Arch Appl Mech (2016) 86:1273–1294
DOI 10.1007/s00419-015-1093-5

ORIGINAL

Zhengwen Jiang · Shui Wan · Zhipeng Zhong · Minghong Li

Geometrically nonlinear analysis for unbalanced adhesively bonded single-lap joint based on flexible interface theory

Received: 30 July 2015 / Accepted: 11 December 2015 / Published online: 22 December 2015

Abstract An improved one-dimensional beam model considering simultaneously the effects of interfacial compliance and the large deflection for adherends and overlap is proposed for the unbalanced single-lap joint (SLJ) under tensile loading. Based on the displacement compatibility condition of flexible interface, the governing differential equations that captured the main features of geometrical nonlinearity for the unbalanced SLJ are derived. The present model can obtain closed-form solutions for edge moment factors, transverse deflections and interface stress distributions for the unbalanced SLJ. The compared results between the present model, existing classical models and nonlinear finite element results validate the accuracy of the geometrically nonlinear model. Finally, the influences of Young's modulus ratio and thickness ratio on the edge moment factors are studied with the present model.

Keywords Unbalanced single-lap joint · Geometrically nonlinear analysis · Flexible interface · Edge moment factor · Interfacial stress

1 Introduction

Due to the outstanding advantages of efficiency and simplicity [1,2], the adhesive bonding technology has been used extensively in aerospace engineering, automotive engineering and civil engineering. The simplest form of the adhesive joint is the single-lap joint (SLJ), which has been incorporated into the ASTM and ISO standards for determining adhesive properties and strength [3]. In order to further understand the interfacial stress distributions and edge moment factors of single-lap joint under tensional load, many studies including the analytical methods [4–8], experimental approaches [2,9–15] and numerical methods [11,14–19] have been conducted on the single-lap joint. Along with the tensional load increases, the phenomenon of large rotation for the single-lap joint will occur and the edge moment factor k will reduce due to the eccentric loading path [20]. Just as Tsai and Morton [1] pointed out the large deflection effect for the adherends cannot be neglected for the long single-lap joint (i.e., $\xi l \geq 1$). Besides the large deflection of the adherends, the overlap geometric

Z. Jiang· S. Wan (✉)
School of Transportation, Southeast University, Nanjing 210096, China
E-mail: seufrpbridge@163.com

Z. Jiang
E-mail: jzhengw@126.com

Z. Zhong
Department of Civil Engineering, Shanxi University, Taiyuan 030013, China

M. Li
School of Civil Engineering, Southeast University, Nanjing 210096, China

nonlinearity also can affect pronouncedly the adhesive stress due to large deflection [21]. Therefore, both the geometric nonlinearity effect of the overlap and the adherends should be taken into account when the geometrically nonlinear analysis for adhesively bonded single-lap joint is performed, i.e., the geometrically nonlinear effect should be incorporated not only to determine the edge moment factor k at the overlap ends but also to construct the equilibrium equations for adherends and adhesive in overlap region [21]. However, once the geometrically nonlinear influence for the bonded region is incorporated into, the analytical solution for the interfacial stress and the edge moment factor will be very difficult [20].

Some analytical models that incorporated only the large deflection effects of adherends have been proposed for the balanced single-lap joint (i.e., the adherends have identical mechanics properties and geometries) [22,23]. Goland and Reissner [24] presented one of the most classical solution for the balanced single-lap joint. In their paper, the large deflection effect of adherends was considered when determining the edge moment factor k. Meanwhile, the influence of the adherends bending and adhesive peel stress was incorporated into the G-R model. Oplinger [25] tried to improve the Hart-Smith model through considering the geometrically nonlinear effect of adherends coupled with the adhesive shear strain. In the Oplinger model, the influence of adhesive thickness deformation was ignored. Compared with the G-R model, Hart-Smith model and the Oplinger model, the L-T model presented more accurate solution for the edge moment factor and adhesive stress due to incorporating simultaneously the effects of the large deflection for overlap and adherends [5,20,26]. Luo and Tong [20] provided the closed-form solutions for the balanced single-lap joint through considering simultaneously adhesive peel stress and shear stress and the large deflection of overlap. Among L-T model, two sets of novel fully coupled nonlinear governing equations for the transverse and longitudinal deflection were constructed using the method of symmetric and antisymmetric deformation superposition. Then, the L-T model was used to solve the problem of the geometrically nonlinear analysis for the composite single-lap joint [5,26]. However, the L-T model is not applicable to the more general unbalanced/unsymmetric single-lap joint (i.e., the adherends have different mechanics properties and/or geometries).

Compared with the balanced single-lap joint, the theoretical analysis of interface stress and edge moment factors for the unbalanced single-lap joint is more complicated due to the fact that the edge loads in two end sections of the overlap region are no more identical and difficult to determine. Some studies conducted the theoretical analysis for the unbalanced single-lap joint. Based on the finite element theory, a one-dimensional beam model considering the effect of the large deflection of adherends was proposed for balanced and unbalanced adhesively bonded single-lap joint by Srinivas [27]. Bigwood and Crocombe presented simplified equations for adhesive stress distributions of unbalanced adhesively bonded single-lap joint based on one-dimensional beam model (i.e., B-C model) [28]. Adams determined the edge moment factors for the unbalanced sing-lap joint considering the necessity of the global equilibrium [29]. Cheng obtained the edge moment factors following the idea of the G-R model, which emphasized the importance of global equilibrium and the deformation compatibility of overlap region after rotation (i.e., Cheng's model) [30]. Meanwhile, the interfacial stresses were obtained using the method of variation principle combined with 2D elasticity theory. Yang and Pang proposed an analytical model for the unbalanced adhesively bonded composite single-lap joint based on the laminated anisotropic theory [31]. Li modified the shear force results of two end sections for the Cheng model using the simplified beam theory [32]. Taheri and Zou [33] provided an analytical solution for the unbalanced single-lap joint based on the adhesive interface constitutive model and the sandwich plate theory. Lee and Kim [34] proposed calculation formulas for the edge moment factor of the unbalanced single-lap joint as neglecting the effect of the transverse shear force. All the aforementioned models for the unbalanced single-lap joint incorporated only the effect of the large deflection for the adherends.

To our best knowledge, there is no closed-form solution for interfacial stress and edge moment factor in the unbalanced single-lap joints when the adhesive strain and the geometrical nonlinear effect of overlap and adherends were considered simultaneously. Meanwhile, the effect of the interfacial compliance on the adhesive stress was neglected in most existing models for the adhesively bonded single-lap joint. Moreover, compared with the balanced single-lap joint, the unbalanced single-lap joint is more widely used. There is significant interest in designing the unbalanced single-lap joint which joins the adherends with different geometries and/or dissimilar materials [32]. Therefore, for further understanding the mechanical property of unbalanced bond single-lap joint and removing the disadvantage of neglecting the effect of the overlap geometric nonlinearity and interfacial compliance, the fully coupled nonlinear analysis is performed using the improved one-dimensional beam model, incorporating simultaneously the effects of interfacial compliance and the large defection for overlap and adherends in this paper. Based on the displacement compatibility condition of the flexible interface theory [35,36], the fully coupled nonlinear governing equations for the transverse and longitudinal deflection of adherends in bonded region are constructed. Then, the closed-form solutions for the interface stress and

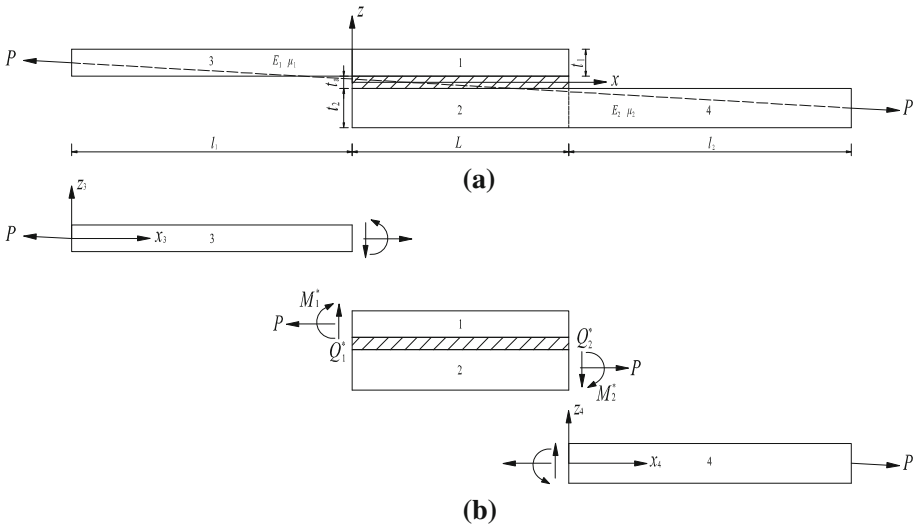

Fig. 1 Schematic configuration for the unbalanced SLJ with tensile load: **a** geometrical parameters; **b** force equilibrium free-body diagram

edge moment factor are obtained. The accuracy of the present solutions is validated through the comparisons with the edge moment factor, adhesive stress and transverse deflection of the nonlinear finite element analysis (i.e., NFEA) and the Cheng's model (or B-C model). Finally, the parametric analysis concerning the edge moment factors is performed.

2 Fully coupled nonlinear analysis

2.1 One-dimensional beam model

Considering the single-lap joint consists of joining adherends with different geometries and/or dissimilar materials, as shown in Fig. 1. The upper adherend with thickness t_1 and the lower adherend with thickness t_2 are bonded by an adhesive layer with thickness t_a. The unbalanced single-lap joint is divided into four sections: the upper adherend (i.e., Sect. 1) and the lower adherend (i.e., Sect. 2), Sects. 3 and 4. The width of the unbalanced SLJ is b. The length of Sects. 3 and 4 are l_1 and l_2, respectively. And the length of bonded region is L. The tensile load acted on the unbalanced single-lap joint is P.

In this study, the basic assumptions adopted are as follows:

1. Both the adhesive layer and two adherends behave linear-elastically.
2. The two adherends and the adhesive layer are boned perfectly.
3. The stress distributions of the adhesive layer are uniform across the thickness.
4. The effects of the large rotation for the adherends and the overlap are incorporated, i.e., the geometrically nonlinear effect should be considered not only to determine the edge moment factor k at the overlap ends but also to construct the equilibrium equations for adherends and adhesive in overlap region. Meanwhile, the assumption of small strain is employed [5,20,26].

The infinitesimal isolated body of the unbalanced SLJ is shown in Fig. 2. By referring to Fig. 2, the following equilibrium equations for the upper adherend and the lower adherend can be obtained as:

$$\frac{\mathrm{d}N_1}{\mathrm{d}x} = b\tau\left(x\right), \quad \frac{\mathrm{d}N_2}{\mathrm{d}x} = -b\tau\left(x\right) \tag{1}$$

$$\frac{\mathrm{d}Q_1}{\mathrm{d}x} = b\sigma\left(x\right) - b\tau\left(x\right)\frac{\mathrm{d}w_1}{\mathrm{d}x}, \quad \frac{\mathrm{d}Q_2}{\mathrm{d}x} = -b\sigma\left(x\right) + b\tau\left(x\right)\frac{\mathrm{d}w_2}{\mathrm{d}x} \tag{2}$$

$$\frac{\mathrm{d}M_1}{\mathrm{d}x} = Q_1 - \frac{bt_1}{2}\tau\left(x\right) + N_1\frac{\mathrm{d}w_1}{\mathrm{d}x}, \frac{\mathrm{d}M_2}{\mathrm{d}x} = Q_2 - \frac{bt_2}{2}\tau\left(x\right) + N_2\frac{\mathrm{d}w_2}{\mathrm{d}x} \tag{3}$$

where N_1 and N_2 are the axial force for the upper adherend and the lower adherend, respectively; Q_1 and Q_2 are the transverse shear force for the upper adherend and the lower adherend, respectively; M_1 and M_2 are the

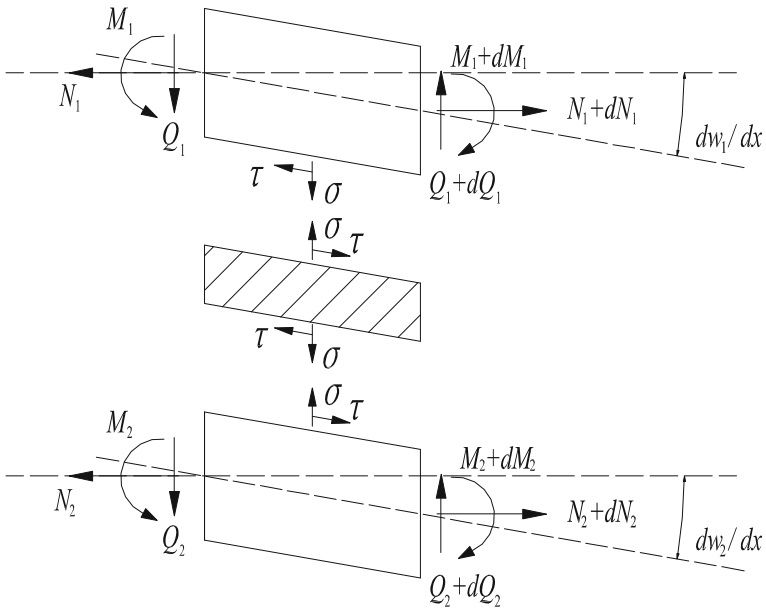

Fig. 2 Stress equilibrium of infinitesimal isolated body for the geometrically nonlinear analysis

bending moment for the upper adherend and the lower adherend, respectively; $\tau\ (x)$ and $\sigma\ (x)$ are shear stress and peel stress for the interface, respectively.

Meanwhile, from Fig. 2, the overall equilibrium of the infinitesimal isolated body can be obtained as:

$$N_T = N_1 + N_2 = P \tag{4}$$

$$Q_T = Q_1 + Q_2 = -Q_1^* = -Q_2^* \tag{5}$$

$$M_T = M_1 + M_2 + N_1 r_1 - N_2 r_2 = P\left[-w - \alpha\left(l_1 + x\right) + r_1\right] \tag{6}$$

where N_T, M_T and Q_T are the total axial force, bending moment and transverse force of the cross section in bonded region, respectively; Q_1^*, Q_2^* are the transverse force in two ends of the bonded region, respectively; r_1 and r_2 are the distance between the neutral planes of bonded region and the upper adherend, and the distance between the neutral planes of bonded region and the lower adherend, respectively; w is the transverse deflection of the bonded region; α is the rotation angle of the SLJ, and $\alpha = (t_1 + 2t_a + t_2)/[2\,(l_1 + L + l_2)]$.

As shown in Fig. 3, r_1 and r_2 can be defined as [32]:

$$r_1 = \frac{t_1 + t_2 + 2t_a}{2\,(1 + A_1/A_2)}; \quad r_2 = \frac{t_1 + t_2 + 2t_a}{2\,(1 + A_2/A_1)} \tag{7}$$

The transverse deflection w of the overlap region can be defined as:

$$w = \frac{w_1 + w_2}{2} \tag{8}$$

Therefore, Eq. (7) can be expressed as:

$$M_T = M_1 + M_2 + N_1 r_1 - N_2 r_2 = P\left[-\frac{w_1 + w_2}{2} - \alpha\left(l_1 + x\right) + r_1\right] \tag{9}$$

Based on the Euler-Bernoulli beam theory, the constitutive equations for the geometrically nonlinear analysis can be expressed as:

$$N_i = A_i\left[\frac{\mathrm{d}u_i}{\mathrm{d}x} + \frac{1}{2}\left(\frac{\mathrm{d}u_i}{\mathrm{d}x}\right)^2 + \frac{1}{2}\left(\frac{\mathrm{d}w_i}{\mathrm{d}x}\right)^2\right] - B_i\frac{d^2 w_i}{\mathrm{d}x^2} \tag{10}$$

$$M_i = B_i\left[\frac{\mathrm{d}u_i}{\mathrm{d}x} + \frac{1}{2}\left(\frac{\mathrm{d}u_i}{\mathrm{d}x}\right)^2 + \frac{1}{2}\left(\frac{\mathrm{d}w_i}{\mathrm{d}x}\right)^2\right] - D_i\frac{d^2 w_i}{\mathrm{d}x^2} \tag{11}$$

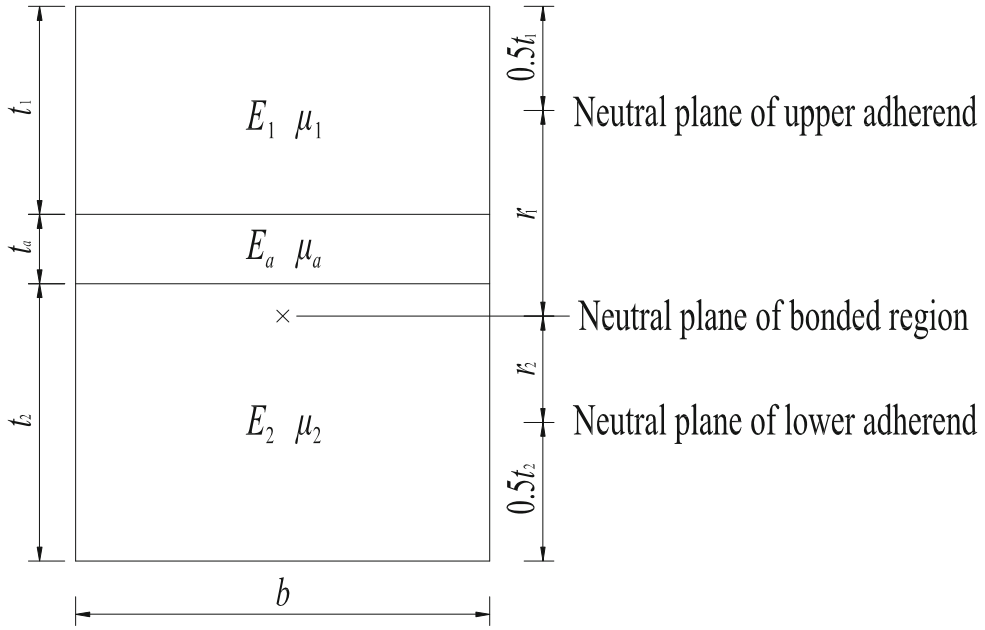

Fig. 3 Neutral plane for the bonded region in unbalanced SLJ

where A_i, B_i and D_i are axial extension, extension bending, and bending stiffness, respectively; for the isotropic beam, $B_i = 0$. By neglecting the nonlinear terms of the Eqs. (10) and (11), the axial force and bending moment of the isotropic beam can be obtained as [20]:

$$N_i = A_i \frac{\mathrm{d}u_i}{\mathrm{d}x}; \quad M_i = -D_i \frac{d^2 w_i}{\mathrm{d}x^2} \qquad (i = 1, 2) \tag{12}$$

2.2 Governing equation

Tsai et al pointed out that the local deformation near free ends of adhesive layer in bonded joint is affected pronouncedly by the highly concentrated shear stress and peel stress of interface [37]. And the influence of the interfacial shear stress and peel stress on the local deformation cannot be neglected. This standpoint has been validated in plated beam using the interface deformable bilayer beam model [35,36]. As shown in Fig. 4, the real deformed cross section for each adherend is nonlinear, which is different from the linear one presumed in the most existing models. Therefore, in order to present an accurate closed-form solution for the unbalanced SLJ, this study will incorporate simultaneously the effects of interface compliance and large deflection, which are not considered in existing models of published literatures.

With referring to Fig. 4, the displacement compatibility conditions for the adhesive interface can be obtained as [35,36]:

$$w_1(x) - C_{n1}\sigma(x) + C_{s1}\tau(x)\frac{\mathrm{d}w_1}{\mathrm{d}x} = w_2(x) + C_{n2}\sigma(x) - C_{s2}\tau(x)\frac{\mathrm{d}w_2}{\mathrm{d}x} + t_a\varepsilon_z(x) \tag{13}$$

$$u_1(x) + \frac{t_1}{2}\frac{\mathrm{d}w_1(x)}{\mathrm{d}x} - C_{s1}\tau(x) = u_2(x) - \frac{t_2}{2}\frac{\mathrm{d}w_2(x)}{\mathrm{d}x} + C_{s2}\tau(x) + t_a\gamma_{xz}(x) \tag{14}$$

$$C_{\mathrm{ni}} = \frac{t_i}{10E_{33}^{(i)}}; \quad C_{\mathrm{si}} = \frac{t_i}{15G_{13}^{(i)}} \tag{15}$$

where C_{ni} and C_{si} $(i = 1, 2)$ are the interfacial compliance coefficients for two adherends under interfacial peel stress and interfacial shear stress, respectively.

The stress–strain relations of the adhesive layer are defined as [5,20,26]:

$$\varepsilon_z(x) = \frac{\sigma(x)}{E_a}; \quad \gamma_{xz}(x) = \frac{\tau(x)}{G_a} \tag{16}$$

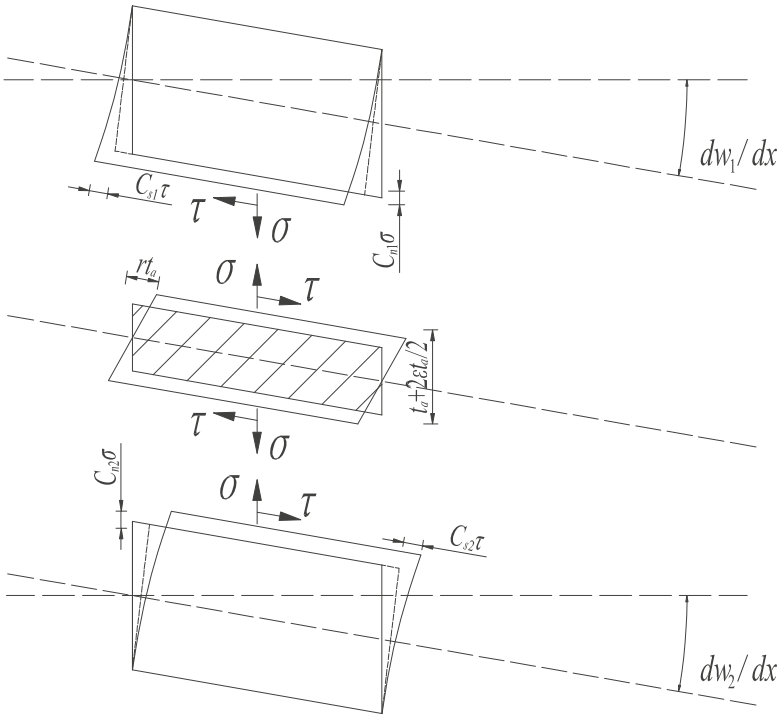

Fig. 4 Displacement continuity condition along interface

Substantial researches have indicated that Eq. (16) is sufficiently accurate for the thin adhesive layer.

The nonlinear terms $\tau\ (x)\ \mathrm{d}w_1/\mathrm{d}x$ and $\tau\ (x)\ \mathrm{d}w_2/\mathrm{d}x$ in Eq. (13) are neglected. Then, differentiating Eq. (13) with respect to x twice and combining with Eq. (16) yield:

$$\frac{d^2w_1\ (x)}{\mathrm{d}x^2} = \frac{d^2w_2\ (x)}{\mathrm{d}x^2} + \left(C_{n1} + C_{n2} + \frac{t_a}{E_a}\right)\frac{d^2\sigma\ (x)}{\mathrm{d}x^2} \tag{17}$$

Substituting Eqs. (1) and (3) into Eq. (2) yields:

$$\sigma\ (x) = \frac{1}{b}\frac{d^2M_1}{\mathrm{d}x^2} + \frac{t_1}{2b}\frac{d^2N_1}{\mathrm{d}x^2} - \frac{N_1}{b}\frac{d^2w_1}{\mathrm{d}x^2};\quad \sigma\ (x) = -\frac{1}{b}\frac{d^2M_2}{\mathrm{d}x^2} + \frac{t_2}{2b}\frac{d^2N_2}{\mathrm{d}x^2} + \frac{N_2}{b}\frac{d^2w_2}{\mathrm{d}x^2} \tag{18}$$

To obtain the closed-form analytical solution for the unbalanced SLJ, the nonlinear terms in Eq. (18) should be linearized. Based on the principle of stiffness distribution, the axial forces N_1 and N_2 of the upper adherend and lower adherend in the boned region are determined as follows:

$$N_1 = \frac{A_1P}{A_1 + A_2};\quad N_2 = \frac{A_2P}{A_1 + A_2} \tag{19}$$

Substituting Eq. (19) into Eq. (18) yields:

$$\begin{cases} \sigma(x) = \frac{1}{b}\frac{d^2M_1}{\mathrm{d}x^2} + \frac{t_1}{2b}\frac{d^2N_1}{\mathrm{d}x^2} - \frac{A_1P}{(A_1+A_2)b}\frac{d^2w_1}{\mathrm{d}x^2} \\ \sigma(x) = -\frac{1}{b}\frac{d^2M_2}{\mathrm{d}x^2} + \frac{t_2}{2b}\frac{d^2N_2}{\mathrm{d}x^2} + \frac{A_2P}{(A_1+A_2)b}\frac{d^2w_2}{\mathrm{d}x^2} \end{cases} \tag{20}$$

Substituting Eqs. (20) and (12) into Eq. (17) and combining with Eqs. (4), (5) and (9) yields:

$$\frac{d^6w_1}{\mathrm{d}x^6} + a_{11}\frac{d^5u_1}{\mathrm{d}x^5} + a_{12}\frac{d^4w_1}{\mathrm{d}x^4} + a_{13}\frac{d^3u_1}{\mathrm{d}x^3} + a_{14}\frac{d^2w_1}{\mathrm{d}x^2} + a_{15}\frac{\mathrm{d}u_1}{\mathrm{d}x} + a_{16}w_1 = f\ (x) \tag{21}$$

where

$$\xi = \frac{D_1}{b}\left(C_{n1} + C_{n2} + \frac{t_a}{E_a}\right);\quad a_{11} = -\frac{t_1A_1}{2D_1};\quad a_{12} = \frac{A_1P}{D_1\ (A_1 + A_2)} - \frac{P}{2D_2};\quad a_{13} = \frac{PA_1t_1}{4D_1D_2};$$

$$a_{14}=\frac{1}{\xi}\left[\left(1+\frac{D_1}{D_2}\right)-\frac{A_1P^2}{2bD_2\left(A_1+A_2\right)}\left(C_{n1}+C_{n2}+\frac{t_a}{E_a}\right)\right];\quad a_{15}=-\frac{1}{\xi}\frac{\left(r_1+r_2\right)A_1}{D_2}a_{16}=-\frac{1}{\xi}\frac{P}{D_2};$$
$$f\left(x\right)=\frac{1}{\xi}\left[\frac{P\alpha}{D_2}\left(l_1+x\right)-\frac{P\left(r_1+r_2\right)}{D_2}\right].$$

Differentiating Eq. (14) with respect to x once and combining with Eqs. (4), (5) and (9) yield:

$$\frac{d^4w_1}{\mathrm{d}x^4}+b_{13}\frac{d^3u_1}{\mathrm{d}x^3}+b_{14}\frac{d^2w_1}{\mathrm{d}x^2}+b_{15}\frac{\mathrm{d}u_1}{\mathrm{d}x}+b_{16}w_1=g\left(x\right)\tag{22}$$

where

$$\eta=\frac{t_2PD_1}{4bD_2}\left(C_{n1}+C_{n2}+\frac{t_a}{E_a}\right);\quad b_{13}=-\frac{1}{\eta}\left[\left(C_{n1}+C_{n2}+\frac{t_a}{E_a}\right)\frac{t_1t_2PA_1}{8bD_2}+\left(C_{s1}+C_{s2}+\frac{t_a}{G_a}\right)\frac{A_1}{b}\right];$$
$$b_{14}=\frac{1}{\eta}\left[\frac{t_2A_1P^2}{4bD_2\left(A_1+A_2\right)}\left(C_{n1}+C_{n2}+\frac{t_a}{E_a}\right)+\left(\frac{t_1}{2}-\frac{D_1t_2}{2D_2}\right)\right];\quad b_{15}=\frac{1}{\eta}\left(1+\frac{A_1}{A_2}+\frac{A_1t_2\left(r_1+r_2\right)}{2D_2}\right);$$
$$b_{16}=\frac{1}{\eta}\frac{t_2P}{2D_2};\quad g\left(x\right)=\frac{1}{\eta}\left[-\frac{t_2}{2D_2}P\alpha\left(l_1+x\right)+\frac{t_2P}{2D_2}\left(r_1+r_2\right)+\frac{P}{A_2}\right].$$

Due to Eqs. (1), (2) and (3) with the geometrically nonlinear character, Eqs. (21) and (22) based on Eqs. (1), (2) and (3) capture the main features of the unbalanced SLJ under static tensile loading. The effects of large deflection are reflected through the terms $a_{12}\left(d^4w_1/\mathrm{d}x^4\right)$, $a_{14}\left(d^2w_1/\mathrm{d}x^2\right)$ in Eq. (21) and terms $b_{14}\left(d^2w_1/\mathrm{d}x^2\right)$ in Eq. (22). Meanwhile, the terms including C_{ni} and C_{si} reflect the effect of interface compliance. That is, the fully coupled nonlinear equations [i.e., Eqs. (21) and (22)] have incorporated simultaneously the influences of the large deflection and the interface compliance.

Eliminating w_1 from the fully coupled nonlinear equations [i.e., Eqs. (21) and (22)] using the elimination method, the differential governing equation for the unbalanced SLJ can be obtained as:

$$\frac{d^9u_1}{\mathrm{d}x^9}+h_{11}\frac{d^7u_1}{\mathrm{d}x^7}+h_{13}\frac{d^5u_1}{\mathrm{d}x^5}+h_{15}\frac{d^3u_1}{\mathrm{d}x^3}+h_{16}\frac{\mathrm{d}u_1}{\mathrm{d}x}=h_{17}g\left(x\right)+h_{18}f\left(x\right)\tag{23}$$

where

$$c_{1i}=\frac{a_{1i}-b_{1(i+2)}}{a_{12}-b_{14}}\left(i=1,3,4\right);\quad c_{1i}=\frac{a_{1i}}{a_{12}-b_{14}}\left(i=5,6\right);\quad c_{17}=\frac{1}{a_{12}-b_{14}};\quad d_{11}=-\frac{c_{11}}{b_{14}-c_{14}};$$
$$d_{1i}=\frac{b_{1i}-c_{1i}}{b_{14}-c_{14}}\left(i=3,5,6\right);\quad d_{17}=\frac{1}{b_{14}-c_{14}};\quad d_{18}=-\frac{c_{17}}{b_{14}-c_{14}};\quad e_{11}=-\frac{d_{11}}{c_{14}-d_{16}};$$
$$e_{1i}=\frac{c_{1(i-2)}-d_{1i}}{c_{14}-d_{16}}\left(i=3,5\right);\quad e_{16}=\frac{c_{15}}{c_{14}-d_{16}};\quad e_{1i}=\frac{c_{1(i-1)}}{c_{14}-d_{16}}\left(i=7,8\right);\quad f_{11}=-\frac{e_{11}}{d_{16}-e_{17}};$$
$$f_{1i}=\frac{d_{1(i-2)}-e_{1i}}{d_{16}-e_{17}}\left(i=3,5\right);\quad f_{16}=\frac{d_{15}-e_{16}}{d_{16}-e_{17}};\quad f_{17}=\frac{d_{17}}{d_{16}-e_{17}};\quad f_{18}=\frac{d_{18}-e_{18}}{d_{16}-e_{17}};\quad g_{11}=-\frac{f_{11}}{e_{17}};$$
$$g_{1i}=\frac{e_{1(i-2)}-f_{1i}}{e_{17}}\left(i=3,5\right);\quad g_{16}=\frac{e_{15}-f_{16}}{e_{17}};\quad g_{17}=\frac{e_{16}}{e_{17}};\quad g_{18}=\frac{e_{18}}{e_{17}}h_{1i}=-\frac{f_{1i}-g_{1(i+2)}}{g_{11}}\left(i=1,3\right);$$
$$h_{1i}=-\frac{f_{1i}-g_{1(i+1)}}{g_{11}}\left(i=5,6\right);\quad h_{17}=-\frac{f_{17}}{g_{11}};\quad h_{18}=-\frac{f_{18}-g_{18}}{g_{11}}$$

and

$$w_1=-g_{11}\frac{d^9u_1}{\mathrm{d}x^9}-g_{13}\frac{d^7u_1}{\mathrm{d}x^7}-g_{15}\frac{d^5u_1}{\mathrm{d}x^5}-g_{16}\frac{d^3u_1}{\mathrm{d}x^3}-g_{17}\frac{\mathrm{d}u_1}{\mathrm{d}x}+g_{18}f\left(x\right)\tag{24}$$

Equations (23) and (24) are valid for the geometrically nonlinear analysis of the general unbalanced single-lap joint. When $a_{12}=0$, $b_{14}=c_{14}$ and $b_{16}=c_{16}$, Eqs. (23) and (24) can be reduced to the balanced SLJ case. Therefore, the differential governing equation for the balanced SLJ can be obtained as:

$$\begin{cases}\frac{d^5u_1}{\mathrm{d}x^5}+d'_{13}\frac{d^3u_1}{\mathrm{d}x^3}+d'_{15}\frac{\mathrm{d}u_1}{\mathrm{d}x}=d'_{17}f\left(x\right)+d'_{18}g\left(x\right)\\ \frac{d^4w_1}{\mathrm{d}x^4}+c_{14}\frac{d^2w_1}{\mathrm{d}x^2}+c_{16}=-c_{11}\frac{d^5u_1}{\mathrm{d}x^5}-c_{13}\frac{d^3u_1}{\mathrm{d}x^3}-c_{15}\frac{\mathrm{d}u_1}{\mathrm{d}x}+c_{17}f\left(x\right)\end{cases}\tag{25}$$

where

$$d'_{1i} = \frac{b_{1i} - c_{1i}}{-c_{11}} \, (i = 3, 5) \, ; \quad d'_{17} = \frac{c_{17}}{c_{11}}; \quad d'_{18} = -\frac{1}{c_{11}}.$$

2.3 Closed-form solutions for the unbalanced SLJ

The characteristic equation of Eq. (23) is:

$$R\left(R^8 + h_{11}R^6 + h_{13}R^4 + h_{15}R^2 + h_{16}\right) = 0 \tag{26}$$

Through numerical calculation, the roots of Eq. (26) can be obtained for one case as: $\pm R_1, \pm R_2, \pm R_3 \pm i\, R_4, 0$.

2.3.1 Deflections for upper adherend

The longitudinal deflection u_1 and transverse deflection w_1 for the upper adherend can be obtained as follows:

$$\begin{aligned} u_1 = {} & c_1 e^{R_1 x} + c_2 e^{-R_1 x} + c_3 e^{R_2 x} + c_4 e^{-R_2 x} + e^{R_3 x} \left[c_5 \cos\left(R_4 x\right) + c_6 \sin\left(R_4 x\right)\right] \\ & + e^{-R_3 x} \left[c_7 \cos\left(R_4 x\right) + c_8 \sin\left(R_4 x\right)\right] + c_9 + u_{1c} \end{aligned} \tag{27}$$

$$\begin{aligned} w_1 = {} & T_1 c_1 e^{R_1 x} + T_2 c_2 e^{-R_1 x} + T_3 c_3 e^{R_2 x} + T_4 c_4 e^{-R_2 x} + e^{R_3 x} \left[T_5 \cos\left(R_4 x\right) + T_6 \sin\left(R_4 x\right)\right] \\ & + e^{-R_3 x} \left[T_7 \cos\left(R_4 x\right) + T_8 \sin\left(R_4 x\right)\right] + w_{1c} \end{aligned} \tag{28}$$

and

$$u_{1c} = \int \left[\frac{h_{17}}{h_{16}} g\left(x\right) + \frac{h_{18}}{h_{16}} f\left(x\right)\right] \mathrm{d}x$$

$$\begin{aligned} S_1 = {} & \left(c_5 R_3^9 + 9c_6 R_3^8 R_4 - 36c_5 R_3^7 R_4^2 - 84c_6 R_3^6 R_4^3 + 126c_5 R_3^5 R_4^4 + 126c_6 R_3^4 R_4^5 - 84c_5 R_3^3 R_4^6 \right. \\ & \left. - 36c_6 R_3^2 R_4^7 + 9c_5 R_3 R_4^8 + c_6 R_4^9\right) \end{aligned}$$

$$\begin{aligned} S_2 = {} & \left(c_6 R_3^9 - 9c_5 R_3^8 R_4 - 36c_6 R_3^7 R_4^2 + 84c_5 R_3^6 R_4^3 + 126c_6 R_3^5 R_4^4 - 126c_5 R_3^4 R_4^5 - 84c_6 R_3^3 R_4^6 \right. \\ & \left. + 36c_5 R_3^2 R_4^7 + 9c_6 R_3 R_4^8 - c_5 R_4^9\right); \end{aligned}$$

$$\begin{aligned} S_3 = {} & \left(-c_7 R_3^9 + 9c_8 R_3^8 R_4 + 36c_7 R_3^7 R_4^2 - 84c_8 R_3^6 R_4^3 - 126c_7 R_3^5 R_4^4 + 126c_8 R_3^4 R_4^5 + 84c_7 R_3^3 R_4^6 \right. \\ & \left. - 36c_8 R_3^2 R_4^7 - 9c_7 R_3 R_4^8 + c_8 R_4^9\right) \end{aligned}$$

$$\begin{aligned} S_4 = {} & \left(-c_8 R_3^9 - 9c_7 R_3^8 R_4 + 36c_8 R_3^7 R_4^2 + 84c_7 R_3^6 R_4^3 - 126c_8 R_3^5 R_4^4 - 126c_7 R_3^4 R_4^5 + 84c_8 R_3^3 R_4^6 \right. \\ & \left. + 36c_7 R_3^2 R_4^7 - 9c_8 R_3 R_4^8 - c_7 R_4^9\right) \end{aligned}$$

$$S_5 = \left(c_5 R_3^7 + 7c_6 R_3^6 R_4 - 21c_5 R_3^5 R_4^2 - 35c_6 R_3^4 R_4^3 + 35c_5 R_3^3 R_4^4 + 21c_6 R_3^2 R_4^5 - 7c_5 R_3 R_4^6 - c_6 R_4^7\right)$$

$$S_6 = \left(c_6 R_3^7 - 7c_5 R_3^6 R_4 - 21c_6 R_3^5 R_4^2 + 35c_5 R_3^4 R_4^3 + 35c_6 R_3^3 R_4^4 - 21c_5 R_3^2 R_4^5 - 7c_6 R_3 R_4^6 + c_5 R_4^7\right)$$

$$S_7 = \left(-c_7 R_3^7 + 7c_8 R_3^6 R_4 + 21c_7 R_3^5 R_4^2 - 35c_8 R_3^4 R_4^3 - 35c_7 R_3^3 R_4^4 + 21c_8 R_3^2 R_4^5 + 7c_7 R_3 R_4^6 - c_8 R_4^7\right)$$

$$S_8 = \left(-c_8 R_3^7 - 7c_7 R_3^6 R_4 + 21c_8 R_3^5 R_4^2 + 35c_7 R_3^4 R_4^3 - 35c_8 R_3^3 R_4^4 - 21c_7 R_3^2 R_4^5 + 7c_8 R_3 R_4^6 + c_7 R_4^7\right)$$

$$S_9 = \left(c_5 R_3^5 + 5c_6 R_3^4 R_4 - 10c_5 R_3^3 R_4^2 - 10c_6 R_3^2 R_4^3 + 5c_5 R_3 R_4^4 + c_6 R_4^5\right);$$

$$S_{10} = \left(c_6 R_3^5 - 5c_5 R_3^4 R_4 - 10c_6 R_3^3 R_4^2 + 10c_5 R_3^2 R_4^3 + 5c_6 R_3 R_4^4 - c_5 R_4^5\right);$$

$$S_{11} = \left(-c_7 R_3^5 + 5c_8 R_3^4 R_4 + 10c_7 R_3^3 R_4^2 - 10c_8 R_3^2 R_4^3 - 5c_7 R_3 R_4^4 + c_8 R_4^5\right);$$

$$S_{12} = \left(-c_8 R_3^5 - 5c_7 R_3^4 R_4 + 10c_8 R_3^3 R_4^2 + 10c_7 R_3^2 R_4^3 - 5c_8 R_3 R_4^4 - c_7 R_4^5\right);$$

$$S_{13} = \left(c_5 R_3^3 + 3c_6 R_3^2 R_4 - 3c_5 R_3 R_4^2 - c_6 R_4^3\right); \quad S_{14} = \left(c_6 R_3^3 - 3c_5 R_3^2 R_4 - 3c_6 R_3 R_4^2 + c_5 R_4^3\right);$$

$$S_{15} = \left(-c_7 R_3^3 + 3c_8 R_3^2 R_4 + 3c_7 R_3 R_4^2 - c_8 R_4^3\right); \quad S_{16} = \left(-c_8 R_3^3 - 3c_7 R_3^2 R_4 + 3c_8 R_3 R_4^2 + c_7 R_4^3\right);$$

$$S_{17} = (c_5 R_3 + c_6 R_4); \; S_{18} = (c_6 R_3 - c_5 R_4); \quad S_{19} = (c_8 R_4 - c_7 R_3); \; S_{20} = -(c_7 R_4 + c_8 R_3)$$

$$T_1 = -\left(g_{11} R_1^9 + g_{13} R_1^7 + g_{15} R_1^5 + g_{16} R_1^3 + g_{17} R_1\right); \quad T_2 = \left(g_{11} R_1^9 + g_{13} R_1^7 + g_{15} R_1^5 + g_{16} R_1^3 + g_{17} R_1\right);$$

$$T_3 = -\left(g_{11} R_2^9 + g_{13} R_2^7 + g_{15} R_2^5 + g_{16} R_2^3 + g_{17} R_2\right); \quad T_4 = \left(g_{11} R_2^9 + g_{13} R_2^7 + g_{15} R_2^5 + g_{16} R_2^3 + g_{17} R_2\right);$$

$$T_5 = -(g_{11} S_1 + g_{13} S_5 + g_{15} S_9 + g_{16} S_{13} + g_{17} S_{17}); \quad T_6 = -(g_{11} S_2 + g_{13} S_6 + g_{15} S_{10} + g_{16} S_{14} + g_{17} S_{18});$$

$$T_7 = -(g_{11} S_3 + g_{13} S_7 + g_{15} S_{11} + g_{16} S_{15} + g_{17} S_{19}); \quad T_8 = -(g_{11} S_4 + g_{13} S_8 + g_{15} S_{12} + g_{16} S_{16} + g_{17} S_{20});$$

$$w_{1c} = -g_{17} \frac{\mathrm{d}u_{1c}}{\mathrm{d}x} + g_{18} f(x)$$

where c_i ($i = 1, 2, \ldots, 9$) are the unknown coefficients determined by the boundary condition and the deformation compatibility conditions; u_{1c} is the particular solution for Eq. (23); w_{1c} is determined by the Eq. (24).

2.3.2 Internal force and moment for upper adherend

By substituting Eqs. (27) and (28) into the Eq. (12) and combining Eqs. (1) and (3), the internal forces N_1, M_1 and Q_1 for the upper adherend can be obtained as:

$$\begin{aligned} N_1 = {} & A_1 c_1 R_1 e^{R_1 x} - A_1 c_2 R_1 e^{-R_1 x} + A_1 c_3 R_2 e^{R_2 x} - A_1 c_4 R_2 e^{-R_2 x} \\ & + e^{R_3 x} \left[A_1 S_{17} \cos(R_4 x) + A_1 S_{18} \sin(R_4 x)\right] + e^{-R_3 x} \left[A_1 S_{19} \cos(R_4 x) + A_1 S_{20} \sin(R_4 x)\right] + N_{1C} \end{aligned} \tag{29}$$

$$\begin{aligned} M_1 = {} & -D_1 T_1 c_1 R_1^2 e^{R_1 x} - D_1 T_2 c_2 R_1^2 e^{-R_1 x} - D_1 T_3 c_3 R_2^2 e^{R_2 x} - D_1 T_4 c_4 R_2^2 e^{-R_2 x} \\ & - e^{R_3 x} \left[U_1 \cos(R_4 x) + U_2 \sin(R_4 x)\right] - e^{-R_3 x} \left[U_3 \cos(R_4 x) + U_4 \sin(R_4 x)\right] \end{aligned} \tag{30}$$

$$\begin{aligned} Q_1 = {} & V_1 e^{R_1 x} + V_2 e^{-R_1 x} + V_3 e^{R_2 x} + V_4 e^{-R_2 x} + e^{R_3 x} \left[V_5 \cos(R_4 x) + V_6 \sin(R_4 x)\right] \\ & + e^{-R_3 x} \left[V_7 \cos(R_4 x) + V_8 \sin(R_4 x)\right] + Q_{1C} \end{aligned} \tag{31}$$

and

$$N_{1C} = A_1 \frac{\mathrm{d}u_{1c}}{\mathrm{d}x};$$

$$U_1 = D_1 \left(T_5 R_3^2 + 2T_6 R_3 R_4 - T_5 R_4^2\right); \quad U_2 = D_1 \left(T_6 R_3^2 - 2T_5 R_3 R_4 - T_6 R_4^2\right);$$

$$U_3 = D_1 \left(T_7 R_3^2 - 2T_8 R_3 R_4 - T_7 R_4^2\right); \quad U_4 = D_1 \left(T_8 R_3^2 + 2T_7 R_3 R_4 - T_8 R_4^2\right);$$

$$V_1 = \left(\frac{t_1}{2} A_1 c_1 R_1^2 - D_1 T_1 c_1 R_1^3 - \frac{P}{2} T_1 c_1 R_1\right); \quad V_2 = \left(D_1 T_2 c_2 R_1^3 + \frac{t_1}{2} A_1 c_2 R_1^2 + \frac{P}{2} T_2 c_2 R_1\right);$$

$$V_3 = \left(\frac{t_1}{2} A_1 c_3 R_2^2 - D_1 T_3 c_3 R_2^3 - \frac{P}{2} T_3 c_3 R_2\right); \quad V_4 = \left(D_1 T_4 c_4 R_2^3 + \frac{t_1}{2} A_1 c_4 R_2^2 + \frac{P}{2} T_4 c_4 R_2\right);$$

$$V_5 = \left[\frac{t_1}{2} (A_1 S_{17} R_3 + A_1 S_{18} R_4) - (U_1 R_3 + U_2 R_4) - \frac{P}{2} (T_5 R_3 + T_6 R_4)\right];$$

$$V_6 = \left[(U_1 R_4 - U_2 R_3) + \frac{t_1}{2} (A_1 S_{18} R_3 - A_1 S_{17} R_4) - \frac{P}{2} (T_6 R_3 - T_5 R_4)\right];$$

$$V_7 = \left[(U_3 R_3 - U_4 R_4) + \frac{t_1}{2} (A_1 S_{20} R_4 - A_1 S_{19} R_3) - \frac{P}{2} (T_8 R_4 - T_7 R_3)\right];$$

$$V_8 = \left[(U_4 R_3 + U_3 R_4) - \frac{t_1}{2} (A_1 S_{20} R_3 + A_1 S_{19} R_4) + \frac{P}{2} (T_8 R_3 + T_7 R_4)\right];$$

$$Q_{1C} = \frac{t_1}{2} A_1 \frac{d^2 u_{1c}}{\mathrm{d}x^2} - \frac{P}{2} \frac{\mathrm{d}w_{1c}}{\mathrm{d}x}$$

2.3.3 Interfacial stress

Substituting Eqs. (28), (29) and (31) into Eqs. (1) and (2) yields:

$$\begin{aligned}\tau(x) = {} & \frac{A_1}{b}c_1R_1^2e^{R_1x} + \frac{A_1}{b}c_2R_1^2e^{-R_1x} + \frac{A_1}{b}c_3R_2^2e^{R_2x} + \frac{A_1}{b}c_4R_2^2e^{-R_2x} \\ & + e^{R_3x}\left[V_9\cos(R_4x) + V_{10}\sin(R_4x)\right] + e^{-R_3x}\left[V_{11}\cos(R_4x) + V_{12}\sin(R_4x)\right] + \tau_C \end{aligned} \tag{32}$$

$$\begin{aligned}\sigma(x) = {} & W_1c_1e^{R_1x} + W_2c_2e^{-R_1x} + W_3c_3e^{R_2x} + W_4c_4e^{-R_2x} \\ & + e^{R_3x}\left[W_5\cos(R_4x) + W_6\sin(R_4x)\right] + e^{-R_3x}\left[W_7\cos(R_4x) + W_8\sin(R_4x)\right] \end{aligned} \tag{33}$$

and

$$V_9 = \frac{A_1}{b}\left(c_5R_3^2 + 2c_6R_3R_4 - c_5R_4^2\right); \quad V_{10} = \frac{A_1}{b}\left(c_6R_3^2 - 2c_5R_3R_4 - c_6R_4^2\right);$$

$$V_{11} = \frac{A_1}{b}\left(c_7R_3^2 - 2c_8R_3R_4 - c_7R_4^2\right); \quad V_{12} = \frac{A_1}{b}\left(c_8R_3^2 + 2c_7R_3R_4 - c_8R_4^2\right); \quad \tau_C = \frac{A_1}{b}\frac{d^2u_{1c}}{dx^2}$$

$$W_1 = \left(\frac{t_1A_1}{2}R_1^3 - \frac{1}{b}D_1T_1R_1^4 - \frac{P}{2b}T_1R_1^2\right); \quad W_2 = -\left(\frac{1}{b}D_1T_2R_1^4 + \frac{t_1A_1}{2}R_1^3 + \frac{P}{2b}T_2R_1^2\right);$$

$$W_3 = \left(\frac{t_1A_1}{2}R_2^3 - \frac{1}{b}D_1T_3R_2^4 - \frac{P}{2b}T_3R_2^2\right); \quad W_4 = -\left(\frac{1}{b}D_1T_4R_2^4 + \frac{t_1A_1}{2}R_2^3 + \frac{P}{2b}T_4R_2^2\right);$$

$$W_5 = \left[\frac{bt_1}{2}\left(V_9R_3 + V_{10}R_4\right) - \frac{1}{b}\left(U_1R_3^2 + 2U_2R_3R_4 - U_1R_4^2\right) - \frac{P}{2b}\left(T_5R_3^2 + 2T_6R_3R_4 - T_5R_4^2\right)\right];$$

$$W_6 = \left[\frac{bt_1}{2}\left(V_{10}R_3 - V_9R_4\right) - \frac{1}{b}\left(U_2R_3^2 - 2U_1R_3R_4 - U_2R_4^2\right) - \frac{P}{2b}\left(T_6R_3^2 - 2T_5R_3R_4 - T_6R_4^2\right)\right];$$

$$W_7 = \left[\frac{1}{b}\left(-U_3R_3^2 + 2U_4R_3R_4 + U_3R_4^2\right) + \frac{bt_1}{2}\left(V_{12}R_4 - V_{11}R_3\right) - \frac{P}{2b}\left(T_7R_3^2 - 2T_8R_3R_4 - T_7R_4^2\right)\right];$$

$$W_8 = \left[\frac{1}{b}\left(-U_4R_3^2 - 2U_3R_3R_4 + U_4R_4^2\right) - \frac{bt_1}{2}\left(V_{12}R_3 + V_{11}R_4\right) - \frac{P}{2b}\left(T_8R_3^2 + 2T_7R_3R_4 - T_8R_4^2\right)\right];$$

2.3.4 Deflections for lower adherend

Substituting Eqs. (27), (28), (32) and (33) into Eqs. (13) and (14) yields:

$$\begin{aligned}w_2 = {} & X_1c_1e^{R_1x} + X_2c_2e^{-R_1x} + X_3c_3e^{R_2x} + X_4c_4e^{-R_2x} \\ & + e^{R_3x}\left[X_5\cos(R_4x) + X_6\sin(R_4x)\right] + e^{-R_3x}\left[X_7\cos(R_4x) + X_8\sin(R_4x)\right] + w_{1c} \end{aligned} \tag{34}$$

$$\begin{aligned}u_2 = {} & X_9c_1e^{R_1x} + X_{10}c_2e^{-R_1x} + X_{11}c_3e^{R_2x} + X_{12}c_4e^{-R_2x} \\ & + e^{R_3x}\left[X_{13}\cos(R_4x) + X_{14}\sin(R_4x)\right] + e^{-R_3x}\left[X_{15}\cos(R_4x) + X_{16}\sin(R_4x)\right] + u_{2C} \end{aligned} \tag{35}$$

and

$$X_1 = \left[T_1 - \left(C_{n1} + C_{n2} + \frac{t_a}{E_a}\right)W_1\right]; \quad X_2 = \left[T_2 - \left(C_{n1} + C_{n2} + \frac{t_a}{E_a}\right)W_2\right];$$

$$X_3 = \left[T_3 - \left(C_{n1} + C_{n2} + \frac{t_a}{E_a}\right)W_3\right]; \quad X_4 = \left[T_4 - \left(C_{n1} + C_{n2} + \frac{t_a}{E_a}\right)W_4\right];$$

$$X_5 = \left[T_5 - \left(C_{n1} + C_{n2} + \frac{t_a}{E_a}\right)W_5\right]; \quad X_6 = \left[T_6 - \left(C_{n1} + C_{n2} + \frac{t_a}{E_a}\right)W_6\right];$$

$$X_7 = \left[T_7 - \left(C_{n1} + C_{n2} + \frac{t_a}{E_a}\right)W_7\right]; \quad X_8 = \left[T_8 - \left(C_{n1} + C_{n2} + \frac{t_a}{E_a}\right)W_8\right];$$

$$X_9 = \left\{1 + \frac{t_1}{2}T_1R_1 + \frac{t_2}{2}\left[T_1 - \left(C_{n1} + C_{n2} + \frac{t_a}{E_a}\right)W_1\right]R_1 - \left(C_{s1} + C_{s2} + \frac{t_a}{G_a}\right)\frac{A_1}{b}R_1^2\right\};$$

$$X_{10}=\left\{1-\frac{t_1}{2}T_2R_1-\frac{t_2}{2}\left[T_2-\left(C_{n1}+C_{n2}+\frac{t_a}{E_a}\right)W_2\right]R_1-\left(C_{s1}+C_{s2}+\frac{t_a}{G_a}\right)\frac{A_1}{b}R_1^2\right\};$$

$$X_{11}=\left\{1+\frac{t_1}{2}T_3R_2+\frac{t_2}{2}\left[T_3-\left(C_{n1}+C_{n2}+\frac{t_a}{E_a}\right)W_3\right]R_2-\left(C_{s1}+C_{s2}+\frac{t_a}{G_a}\right)\frac{A_1}{b}R_2^2\right\};$$

$$X_{12}=\left\{1-\frac{t_1}{2}T_4R_2-\frac{t_2}{2}\left[T_4-\left(C_{n1}+C_{n2}+\frac{t_a}{E_a}\right)W_4\right]R_2-\left(C_{s1}+C_{s2}+\frac{t_a}{G_a}\right)\frac{A_1}{b}R_2^2\right\};$$

$$\begin{aligned}X_{13}=c_5+\frac{t_1}{2}(T_5R_3+T_6R_4)+\frac{t_2}{2}\Bigg[&T_5R_3-\left(C_{n1}+C_{n2}+\frac{t_a}{E_a}\right)R_3W_5+T_6R_4\\&-\left(C_{n1}+C_{n2}+\frac{t_a}{E_a}\right)R_4W_6\Bigg]-\left(C_{s1}+C_{s2}+\frac{t_a}{G_a}\right)V_9;\end{aligned}$$

$$\begin{aligned}X_{14}=c_6+\frac{t_1}{2}(T_6R_3-T_5R_4)+\frac{t_2}{2}\Bigg[&T_6R_3-\left(C_{n1}+C_{n2}+\frac{t_a}{E_a}\right)R_3W_6-T_5R_4\\&+\left(C_{n1}+C_{n2}+\frac{t_a}{E_a}\right)R_4W_5\Bigg]-\left(C_{s1}+C_{s2}+\frac{t_a}{G_a}\right)V_{10};\end{aligned}$$

$$\begin{aligned}X_{15}=c_7+\frac{t_1}{2}(T_8R_4-T_7R_3)+\frac{t_2}{2}\Bigg[&T_8R_4-\left(C_{n1}+C_{n2}+\frac{t_a}{E_a}\right)R_4W_8-T_7R_3\\&+\left(C_{n1}+C_{n2}+\frac{t_a}{E_a}\right)R_3W_7\Bigg]-\left(C_{s1}+C_{s2}+\frac{t_a}{G_a}\right)V_{11};\end{aligned}$$

$$\begin{aligned}X_{16}=c_8-\frac{t_1}{2}(T_8R_3+T_7R_4)+\frac{t_2}{2}\Bigg[&-T_8R_3+\left(C_{n1}+C_{n2}+\frac{t_a}{E_a}\right)R_3W_8-T_7R_4\\&+\left(C_{n1}+C_{n2}+\frac{t_a}{E_a}\right)R_4W_7\Bigg]-\left(C_{s1}+C_{s2}+\frac{t_a}{G_a}\right)V_{12};\end{aligned}$$

$$u_{2C}=c_9+u_{1c}+\frac{t_1+t_2}{2}\frac{\mathrm{d}w_{1c}}{\mathrm{d}x}-\left(C_{s1}+C_{s2}+\frac{t_a}{G_a}\right)\tau_C$$

2.3.5 Internal force and moment for lower adherend

By substituting Eqs. (34) and (35) into the Eq. (12) and combining Eqs. (1) and (3), the internal forces N_2, M_2 and Q_2 for the lower adherend can be obtained as:

$$\begin{aligned}M_2=-D_2\frac{d^2w_2}{\mathrm{d}x^2}=&Y_1c_1e^{R_1x}+Y_2c_2e^{-R_1x}+Y_3c_3e^{R_2x}+Y_4c_4e^{-R_2x}\\&+e^{R_3x}\left[Y_5\cos(R_4x)+Y_6\sin(R_4x)\right]+e^{-R_3x}\left[Y_7\cos(R_4x)+Y_8\sin(R_4x)\right]\end{aligned}\tag{36}$$

$$\begin{aligned}N_2=&A_2X_9R_1c_1e^{R_1x}-A_2X_{10}R_1c_2e^{-R_1x}+A_2X_{11}R_2c_3e^{R_2x}-A_2X_{12}R_2c_4e^{-R_2x}\\&+e^{R_3x}\left[Y_9\cos(R_4x)+Y_{10}\sin(R_4x)\right]+e^{-R_3x}\left[Y_{11}\cos(R_4x)+Y_{12}\sin(R_4x)\right]+N_{2C}\end{aligned}\tag{37}$$

$$\begin{aligned}Q_2=&Z_1c_1e^{R_1x}+Z_2c_2e^{-R_1x}+Z_3c_3e^{R_2x}+Z_4c_4e^{-R_2x}\\&+e^{R_3x}\left[Z_5\cos(R_4x)+Z_6\sin(R_4x)\right]+e^{-R_3x}\left[Z_7\cos(R_4x)+Z_8\sin(R_4x)\right]+Q_{2C}\end{aligned}\tag{38}$$

and

$$Y_1=-D_2\left[T_1-\left(C_{n1}+C_{n2}+\frac{t_a}{E_a}\right)W_1\right]R_1^2;\quad Y_2=-D_2\left[T_2-\left(C_{n1}+C_{n2}+\frac{t_a}{E_a}\right)W_2\right]R_1^2;$$

$$Y_3=-D_2\left[T_3-\left(C_{n1}+C_{n2}+\frac{t_a}{E_a}\right)W_3\right]R_2^2;\quad Y_4=-D_2\left[T_4-\left(C_{n1}+C_{n2}+\frac{t_a}{E_a}\right)W_4\right]R_2^2;$$

$$Y_5=-D_2\left[\begin{array}{l}T_5R_3^2-\left(C_{n1}+C_{n2}+\frac{t_a}{E_a}\right)R_3^2W_5+2T_6R_3R_4-2\left(C_{n1}+C_{n2}+\frac{t_a}{E_a}\right)R_3R_4W_6\\\quad+\left(C_{n1}+C_{n2}+\frac{t_a}{E_a}\right)R_4^2W_5-T_5R_4^2\end{array}\right];$$

$$Y_6 = -D_2 \begin{bmatrix} T_6 R_3^2 - \left(C_{n1} + C_{n2} + \frac{t_a}{E_a}\right) R_3^2 W_6 - 2T_5 R_3 R_4 + 2\left(C_{n1} + C_{n2} + \frac{t_a}{E_a}\right) R_3 R_4 W_5 \\ + \left(C_{n1} + C_{n2} + \frac{t_a}{E_a}\right) R_4^2 W_6 - T_6 R_4^2 \end{bmatrix};$$

$$Y_7 = -D_2 \begin{bmatrix} +T_7 R_3^2 - \left(C_{n1} + C_{n2} + \frac{t_a}{E_a}\right) R_3^2 W_7 - 2T_8 R_3 R_4 + 2\left(C_{n1} + C_{n2} + \frac{t_a}{E_a}\right) R_3 R_4 W_8 \\ + \left(C_{n1} + C_{n2} + \frac{t_a}{E_a}\right) R_4^2 W_7 - T_7 R_4^2 \end{bmatrix};$$

$$Y_8 = -D_2 \begin{bmatrix} +T_8 R_3^2 - \left(C_{n1} + C_{n2} + \frac{t_a}{E_a}\right) R_3^2 W_8 + 2T_7 R_3 R_4 - 2\left(C_{n1} + C_{n2} + \frac{t_a}{E_a}\right) R_3 R_4 W_7 \\ + \left(C_{n1} + C_{n2} + \frac{t_a}{E_a}\right) R_4^2 W_8 - T_8 R_4^2 \end{bmatrix};$$

$$Y_9 = A_2 (X_{13} R_3 + X_{14} R_4); \quad Y_{10} = A_2 (X_{14} R_3 - X_{13} R_4); Y_{11} = A_2 (X_{16} R_4 - X_{15} R_3);$$

$$Y_{12} = -A_2 (X_{16} R_3 + X_{15} R_4); N_{2C} = A_2 \frac{\mathrm{d}u_{2C}}{\mathrm{d}x};$$

$$Z_1 = \left\{ Y_1 R_1 + \frac{t_2 A_1}{2} R_1^2 - \frac{P}{2}\left[T_1 - \left(C_{n1} + C_{n2} + \frac{t_a}{E_a}\right) W_1\right] R_1 \right\};$$

$$Z_2 = \left\{ \frac{t_2 A_1}{2} R_1^2 - Y_2 R_1 - \frac{P}{2}\left[T_2 - \left(C_{n1} + C_{n2} + \frac{t_a}{E_a}\right) W_2\right] R_1 \right\};$$

$$Z_3 = \left\{ Y_3 R_2 + \frac{t_2 A_1}{2} R_2^2 - \frac{P}{2}\left[T_3 - \left(C_{n1} + C_{n2} + \frac{t_a}{E_a}\right) W_3\right] R_2 \right\};$$

$$Z_4 = \left\{ \frac{t_2 A_1}{2} R_2^2 - Y_4 R_2 - \frac{P}{2}\left[T_4 - \left(C_{n1} + C_{n2} + \frac{t_a}{E_a}\right) W_4\right] R_2 \right\};$$

$$Z_5 = (Y_5 R_3 + Y_6 R_4) + \frac{bt_2}{2} V_9 - \frac{P}{2}\left[T_5 R_3 - \left(C_{n1} + C_{n2} + \frac{t_a}{E_a}\right) R_3 W_5 + T_6 R_4 - \left(C_{n1} + C_{n2} + \frac{t_a}{E_a}\right) R_4 W_6\right];$$

$$Z_6 = (Y_6 R_3 - Y_5 R_4) + \frac{bt_2}{2} V_{10} - \frac{P}{2}\left[T_6 R_3 - \left(C_{n1} + C_{n2} + \frac{t_a}{E_a}\right) R_3 W_6 - T_5 R_4 + \left(C_{n1} + C_{n2} + \frac{t_a}{E_a}\right) R_4 W_5\right];$$

$$Z_7 = (Y_8 R_4 - Y_7 R_3) + \frac{bt_2}{2} V_{11} - \frac{P}{2}\left[T_8 R_4 - \left(C_{n1} + C_{n2} + \frac{t_a}{E_a}\right) R_4 W_8 - T_7 R_3 + \left(C_{n1} + C_{n2} + \frac{t_a}{E_a}\right) R_3 W_7\right];$$

$$Z_8 = \frac{bt_2}{2} V_{12} - (Y_8 R_3 + Y_7 R_4) - \frac{P}{2}\left[-T_8 R_3 + \left(C_{n1} + C_{n2} + \frac{t_a}{E_a}\right) R_3 W_8 - T_7 R_4 + \left(C_{n1} + C_{n2} + \frac{t_a}{E_a}\right) R_4 W_7\right];$$

$$Q_{2C} = \frac{bt_2}{2} \tau_C - \frac{P}{2} \frac{\mathrm{d}w_{1c}}{\mathrm{d}x}$$

2.3.6 Deflections for the outer adherend

Based on the classical beam theory, the governing equations for the region 3 and region 4 can be obtained as [20]:

$$\begin{cases} A_1 \frac{\mathrm{d}u_3}{\mathrm{d}x_3} = P \\ -D_1 \frac{d^2 w_3}{\mathrm{d}x_3^2} = P(-w_3 - \alpha x_3) \end{cases} \quad (0 \le x_3 \le l_1) \tag{39}$$

$$\begin{cases} A_2 \frac{\mathrm{d}u_4}{\mathrm{d}x_4} = P \\ -D_2 \frac{d^2 w_4}{\mathrm{d}x_4^2} = P\left[-w_4 - \alpha\left(l_1 + L + x_4\right) + \frac{t_1+t_2+2t_a}{2}\right] \end{cases} \quad (0 \le x_4 \le l_2) \tag{40}$$

The boundary conditions for the region 3 and region 4 can be expressed as:

$$\begin{cases} x_3 = 0 \; u_3 = 0, w_3 = 0 \\ x_3 = l_1 \; -D_1 \frac{d^2 w_3}{\mathrm{d}x_3^2} = -M_1^* \end{cases}; \quad \begin{cases} x_4 = 0 \; -D_2 \frac{d^2 w_4}{\mathrm{d}x_4^2} = M_2^* \\ x_4 = l_2 \; w_4 = 0 \end{cases} \tag{41}$$

In terms of Eqs. (41), (39) and (40) are solved and the deflections for the outer adherends can be obtained as:

$$\begin{cases} u_3 = \frac{P}{A_1} x_3 \\ w_3 = \frac{M_1^* \sinh(\beta_1 x_3)}{P \sinh(\beta_1 l_1)} - \alpha x_3 \end{cases} \quad (0 \le x_3 \le l_1) \tag{42}$$

$$\begin{cases} u_4 = \frac{P}{A_2} x_4 + C \\ w_4 = -\frac{M_2^*}{P} \cosh(\beta_2 x_4) + \\ \frac{M_2^*}{P} \coth(\beta_2 l_2) \sinh(\beta_2 x_4) + \frac{t_1+t_2+2t_a}{2} - \alpha\left(l_1 + L + x_4\right) \end{cases} \quad (0 \le x_4 \le l_2) \tag{43}$$

where $\beta_1 = \sqrt{P/D_1}$; $\beta_2 = \sqrt{P/D_2}$.

2.3.7 Boundary condition

The unknown coefficients c_1, c_2, c_3, c_4, c_5, c_6, c_7, c_8, c_9 and the edge moments M_1^*, M_2^*, Q_1^*, Q_2^* can be determined by following boundary conditions, deformation compatibility conditions and global equilibrium conditions:

$$N_1(0) = P, \quad Q_1(0) = -Q_1^*, \quad M_1(0) = -M_1^* \tag{44}$$

$$N_2(L) = P, \quad Q_2(L) = -Q_2^*, \quad M_2(L) = M_2^* \tag{45}$$

$$w_1|_{x=0} = w_3|_{x_3=l_1}, \left.\frac{\mathrm{d}w_1}{\mathrm{d}x}\right|_{x=0} = \left.\frac{\mathrm{d}w_3}{\mathrm{d}x_3}\right|_{x_3=l_1} \tag{46}$$

$$w_2|_{x=L} = w_4|_{x_4=0}, \left.\frac{\mathrm{d}w_2}{\mathrm{d}x}\right|_{x=L} = \left.\frac{\mathrm{d}w_4}{\mathrm{d}x_4}\right|_{x_4=0} \tag{47}$$

$$u_1|_{x=0} = u_3|_{x_3=l_1} \tag{48}$$

$$Q_1^* = Q_2^* = \frac{1}{L}\left[\frac{P\left(t_1 + t_2 + 2t_a\right)}{2} - M_1^* - M_2^*\right] \tag{49}$$

The coefficients c_1, c_2, c_3, c_4, c_5, c_6, c_7, c_8, c_9 and M_1^*, M_2^*, Q_1^* and Q_2^* can be determined through solving Eqs. (44)–(49). Then, the edge moment factor k_1 *and* k_2 can be obtained as follows:

$$k_1 = \frac{2M_1^*}{P\left(t_1 + t_a\right)}, \quad k_2 = \frac{2M_2^*}{P\left(t_2 + t_a\right)} \tag{50}$$

3 Verification and discussion

In order to validate the applicability and accuracy of the present model, the edge moment factors, the transverse deflections of bonded region and interfacial stress distributions for the unbalanced SLJ are determined with four different methods (i.e., the present model, nonlinear finite element analysis (NFEA), Cheng's model or B-C model) in this section. Then, the comparisons among the solutions of the four different models are conducted. The geometrical parameters and material properties for the unbalanced SLJ are shown in Table 1. In case 1, 2 and 3, $E_a/E_1 = 0.01$, 0.05 and 0.1 corresponding to flexible, semiflexible and inflexible adhesive materials, respectively.

Table 1 Material properties and geometrical parameters for unbalanced SLJ

Case	Material properties			Geometrical parameters	P (N)
	Upper adherend	Lower adherend	Adhesive layer		
1	$E_1 = 70\,\text{GPa},\ \nu_1 = 0.34$	$E_2 = 140\,\text{GPa},\ \nu_2 = 0.34$	$E_a = 0.7\,\text{GPa},\ \nu_a = 0.4$	$l_1 = l_2 = 40\,\text{mm},\ t_1 = t_2 = 2\,\text{mm},\ t_a = 0.2\,\text{mm},\ b = 1\,\text{mm}$	600
2	$E_1 = 70\,\text{GPa},\ \nu_1 = 0.34$	$E_2 = 280\,\text{GPa},\ \nu_2 = 0.34$	$E_a = 3.5\,\text{GPa},\ \nu_a = 0.4$	$l_1 = l_2 = 20\,\text{mm},\ t_1 = 2\,\text{mm},\ t_2 = 1\,\text{mm},\ t_a = 0.2\,\text{mm},\ b = 1\,\text{mm}$	600
3	$E_1 = 70\,\text{GPa},\ \nu_1 = 0.34$	$E_2 = 35\,\text{GPa},\ \nu_2 = 0.34$	$E_a = 7.0\,\text{GPa},\ \nu_a = 0.4$	$l_1 = l_2 = 80\,\text{mm},\ t_1 = 2\,\text{mm},\ t_2 = 3\,\text{mm},\ t_a = 0.2\,\text{mm},\ b = 1\,\text{mm}$	500

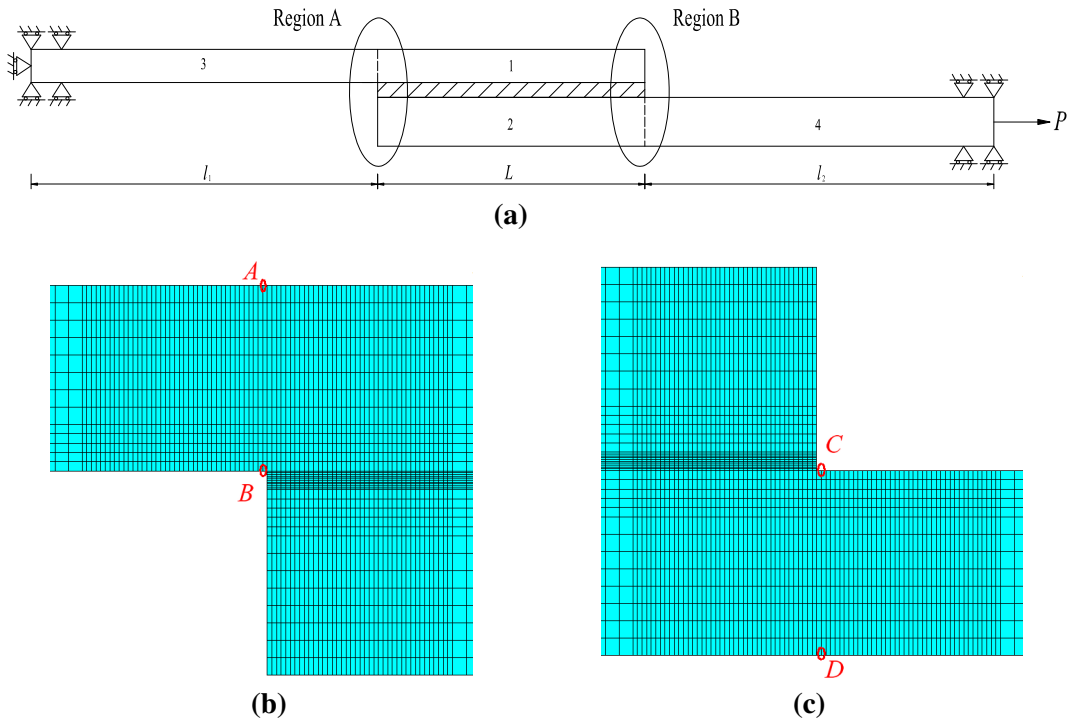

Fig. 5 Boundary conditions and refined mesh near two free ends of adhesive layer for unbalanced SLJ: **a** boundary condition; **b** refined mesh for region A; **c** refined mesh for region B

3.1 Finite element model

The geometrically nonlinear finite element model for the unbalanced SLJ under the static tensile loading is conducted with the finite element software ANSYS. The loading and boundary conditions for the typical FE model are shown in Fig. 5a. Two adherends and the adhesive layer are meshed by the 2D plane strain eight-node element (i.e., Plane82 element), which has large deflection capability. The material linearity is employed in the geometrically nonlinear finite element model. In order to determine accurately the peak interface stresses near two free ends of the adhesive layer, a very fine mesh with the smallest element of dimensions 0.05 mm × 0.02 mm is used to mesh region A and region B, as shown in Fig. 5b. The adhesive layer is divided into 10 sections along its thickness. During the geometrically nonlinear analysis for the typical FE model, the Newton's method is used and 40 equal load increments are employed. Based on the stress results using the NFEA, the edge moment factors for the unbalanced SLJ can be determined as follows [11,29,38]:

$$\begin{cases} \sigma_{\text{bending1}} = \frac{\sigma_B - \sigma_A}{2},\ M_1^{NF} = \frac{bt_1^2\sigma_{\text{bending1}}}{6},\ k_1^{NF} = \frac{bt_1^2\sigma_{\text{bending1}}}{3P(t_1+t_a)} \\ \sigma_{\text{bending2}} = \frac{\sigma_C - \sigma_D}{2},\ M_2^{NF} = \frac{bt_2^2\sigma_{\text{bending2}}}{6},\ k_2^{NF} = \frac{bt_2^2\sigma_{\text{bending2}}}{3P(t_2+t_a)} \end{cases} \tag{51}$$

where σ_A, σ_B,σ_C and σ_D are the longitudinal stresses of top/bottom surface points A, B, C and D, which are shown in Fig. 5b, c; σ_{bending1} and σ_{bending2} are bending stresses at two edge sections for the bonded region, respectively; M_1^{NF}, M_2^{NF} are bending moments at two edge sections for the bonded region, respectively; k_1^{NF} and k_2^{NF} are bending moment factors at two edge sections for the bonded region, respectively.

3.2 Results and discussion

The edge moment factors for the unbalanced SLJ under static tensile loading obtained with the present model, Cheng's model and NFEA are presented along the parameter $\beta_1(L/2)$ in Figs. 6, 7 and 8. Similarly, the

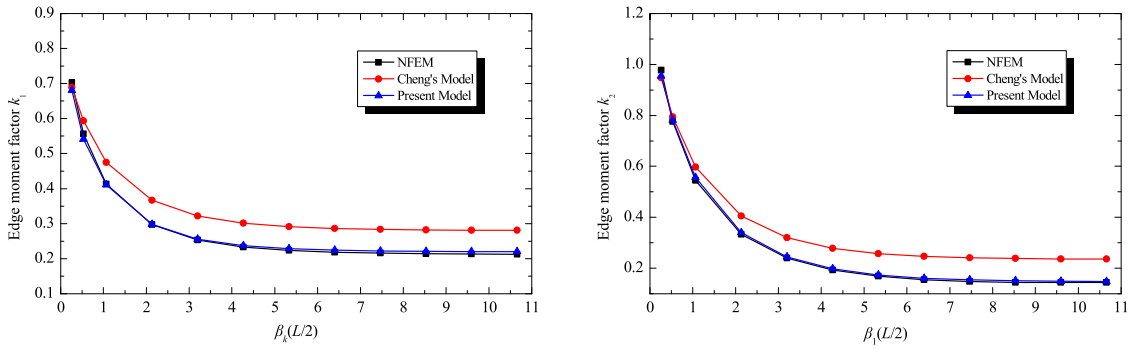

Fig. 6 Edge moment factors for unbalanced SLJ under case 1: **a** edge moment factor k_1; **b** edge moment factor k_2

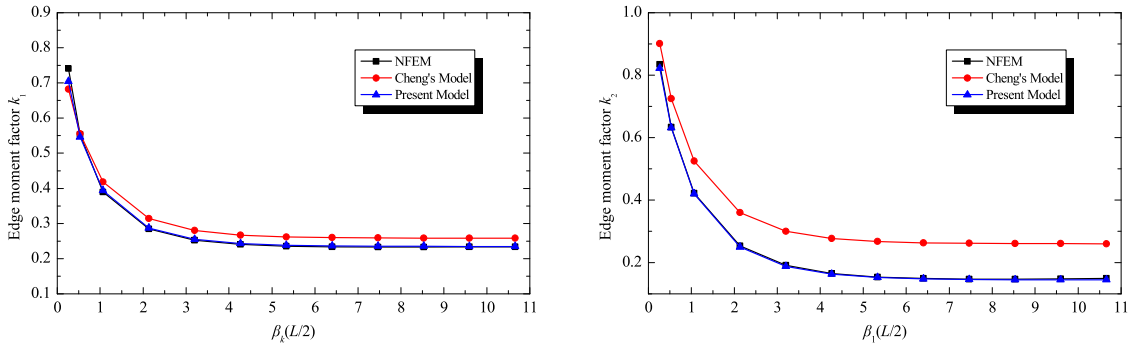

Fig. 7 Edge moment factors for unbalanced SLJ under case 2: **a** edge moment factor k_1; **b** edge moment factor k_2

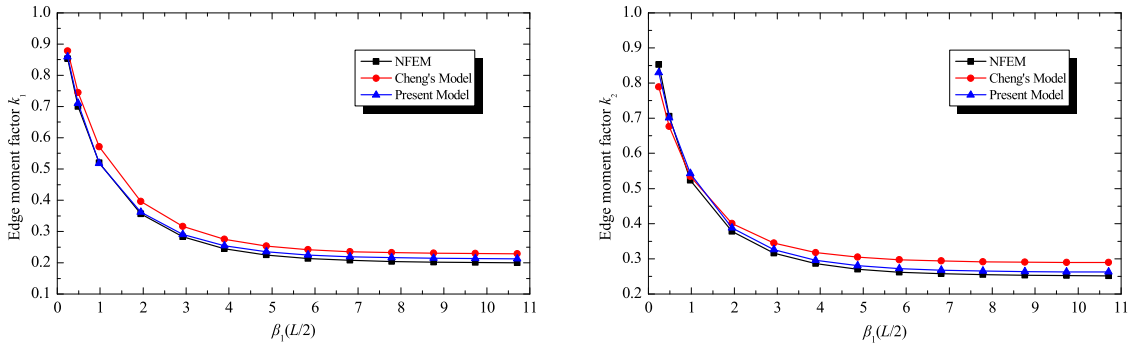

Fig. 8 Edge moment factors for unbalanced SLJ under case 3: **a** edge moment factor k_1; **b** edge moment factor k_2

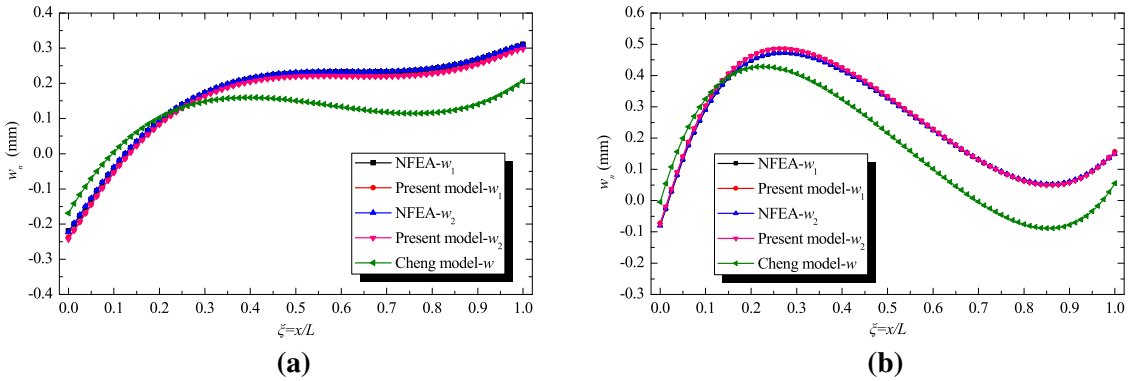

Fig. 9 Transverse deflections for unbalanced SLJ under case 1: **a** $L = 100$; **b** $L = 200$

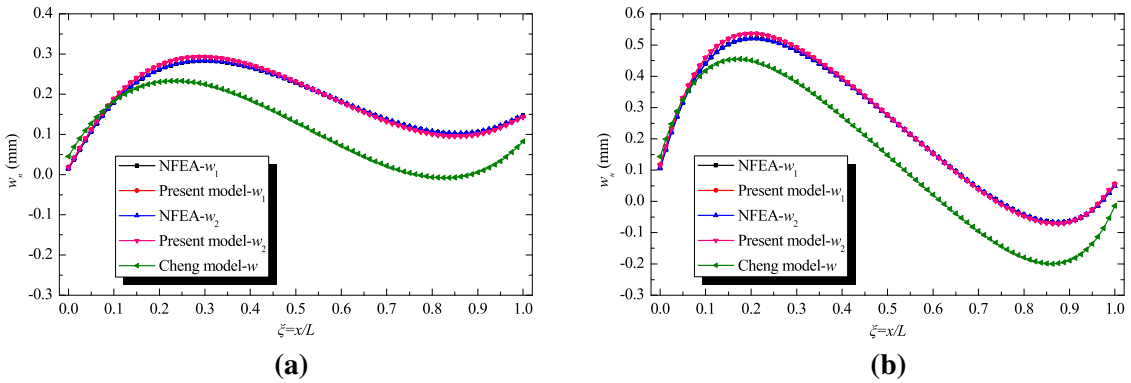

Fig. 10 Transverse deflections for unbalanced SLJ under case 2: **a** $L = 100$; **b** $L = 200$

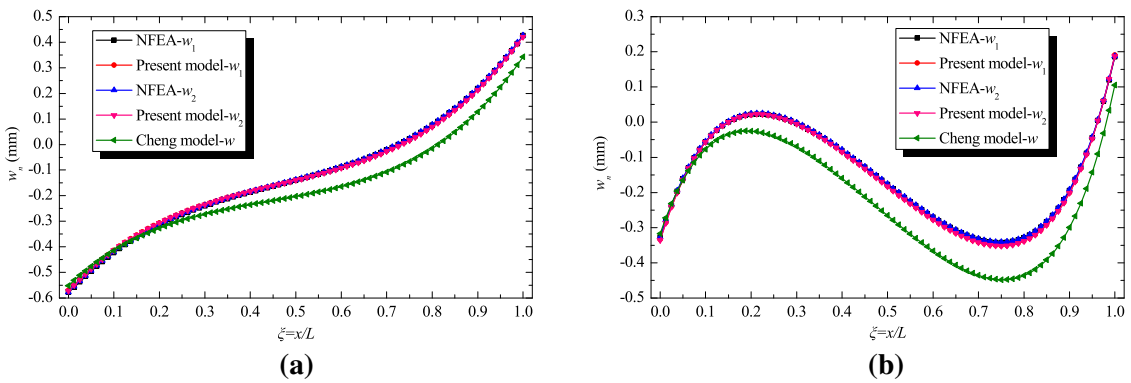

Fig. 11 Transverse deflections for unbalanced SLJ under case 3: **a** $L = 100$; **b** $L = 220$

transverse deflections of the overlap region and interfacial stress components in the middle plane of adhesive layer for the unbalanced SLJ determined with the present model, Cheng's model (or B-C model) and NFEA are presented along the normalized bonded length (i.e., $\xi = x/L$) in Figs. 9, 10, 11, 12, 13 and 14.

3.2.1 Edge moment factors

The edge moment factors for the unbalanced SLJ under case 1, 2 and 3 are shown in Figs. 6, 7 and 8. From Figs. 6, 7 and 8, it can be noted that the edge moment factors k_1 and k_2 decrease as $\beta_1(L/2)$ increases gradually. This phenomenon is induced by the eccentric loading path of unbalanced SLJ. Meanwhile, the edge moment factors determined by the present model agree extremely well with the results of NFEA. The relative errors

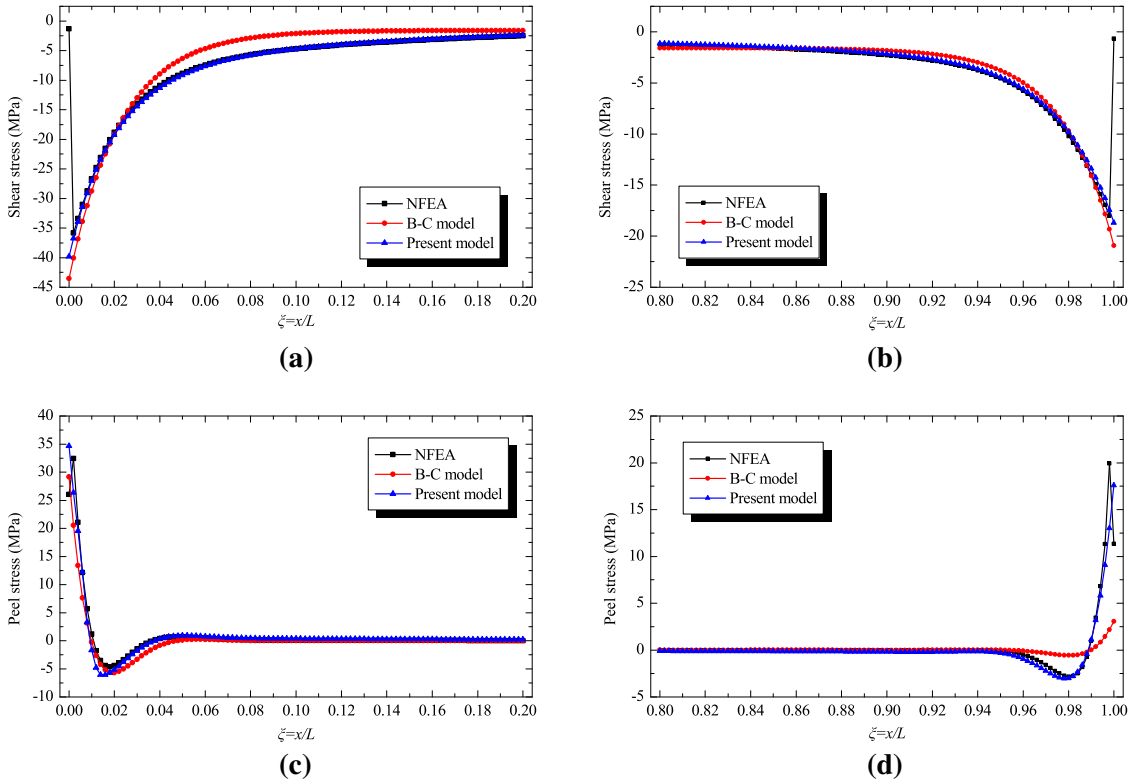

Fig. 12 Interfacial stresses for unbalanced SLJ with $L = 200$ under case 1: **a** shear stress along $0 \leq \xi \leq 0.2$; **b** peel stress along $0 \leq \xi \leq 0.2$; **c** shear stress along $0.8 \leq \xi \leq 1.0$; **d** peel stress along $0.8 \leq \xi \leq 1.0$

between the present model and NFEA are <7 %. Comparatively speaking, the results predicted by the Cheng's model have more deviations, especially for the long SLJ (i.e., $\beta_1(L/2) \geq 1$). The most relative error between the Cheng's model and NFEA is more than 30 % for the unbalanced long SLJ under case 1. The excessive deviation is due to the fact that the geometric nonlinear effect of the overlap is neglected when the Cheng's model determined the edge moment factors. And the present model obtains the edge moment factors through considering simultaneously the effects of the interfacial compliance and the large deflection for the overlap and the adherends. That is, for the long unbalanced SLJ, the effects of the interfacial compliance and the large deflection of the overlap region and the adherends cannot be neglected when the edge moment factors are determined. Therefore, the present model considering simultaneously the geometrically nonlinear effect and the interface compliance can predict accurately the edge moment factors for the unbalanced SLJ, whatever the SLJ composed of flexible, semiflexible and inflexible adhesive layer.

3.2.2 Transverse deflections for bonded region

From Figs. 9, 10 and 11, it can be obtained that the transverse deflections in overlap region of the long unbalanced SLJ predicted by the present model correlate extremely well with the results of the NFEA under case 1, 2 and 3. Both the present analysis and the NFEA are the displacement-based solutions. The good agreement in transverse deflections of the upper and lower adherend between the results predicted by present model and the NFEA indicates vividly that the governing Eqs. (23) and (24) capture the main features of the geometrically nonlinearity for the unbalanced SLJ under static tensile load. Comparatively speaking, the Cheng's model which neglected the geometrically nonlinear effect of the overlap predicted the transverse deflections of overlap regions for the long unbalanced SLJ with large deviations. Therefore, the effects of the interfacial compliance and the large deflection for the overlap and the adherends should not be neglected when the transverse deflections of the overlap regions are determined.

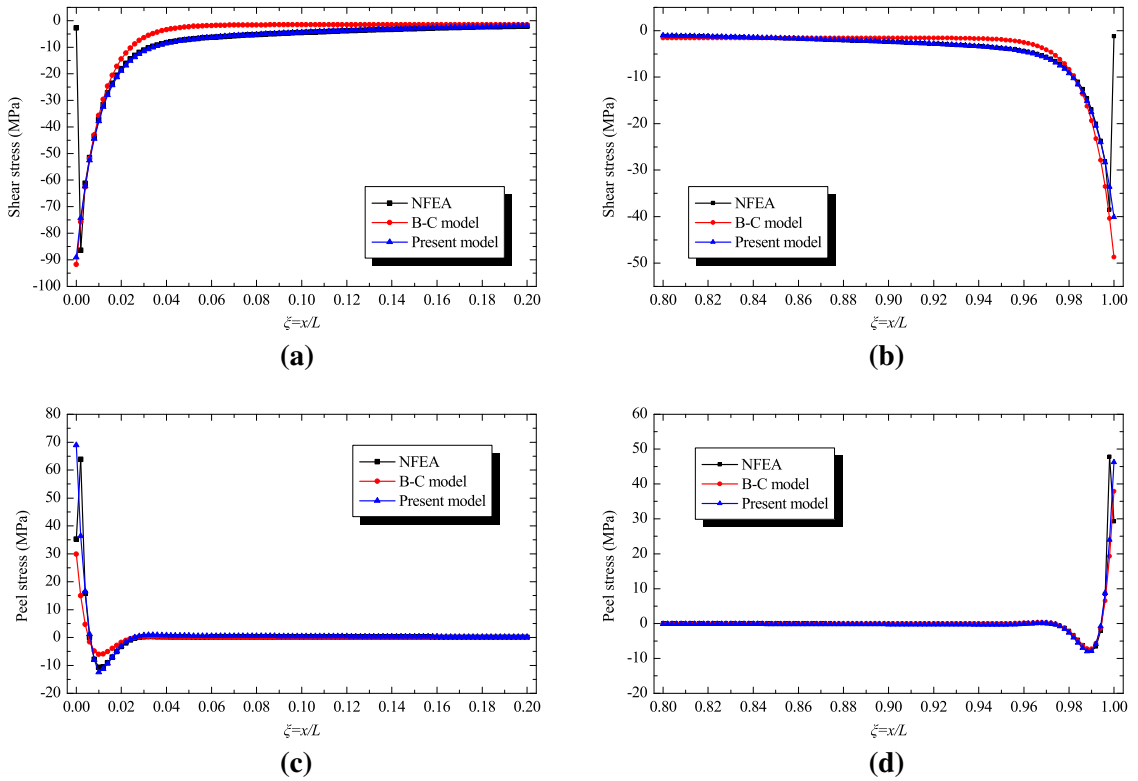

Fig. 13 Interfacial stresses for unbalanced SLJ with $L = 200$ under case 2: **a** shear stress along $0 \leq \xi \leq 0.2$; **b** peel stress along $0 \leq \xi \leq 0.2$; **c** shear stress along $0.8 \leq \xi \leq 1.0$; **d** peel stress along $0.8 \leq \xi \leq 1.0$

3.2.3 Interfacial stress

In Figs. 12, 13 and 14, the comparisons for the shear stresses and peel stresses of adhesive interface in the regions of $0 \leq \xi \leq 0.2$ and $0.8 \leq \xi \leq 1.0$ are presented. Due to the fact that the present model and B-C model have the disadvantage of neglecting the variation of adhesive stresses through the thickness, the adhesive stresses at middle plane are chosen for the results of NFEA, where the stress distribution is variable across the thickness. From Figs. 12a, c, 13a, c and 14a, c, it can be obtained that the interfacial shear stresses of two free ends determined by NFEA approach zero after reaching the peak values near the two free ends. The present model and B-C model based on the one-dimensional beam theory cannot model the edge stress-free conditions, which can be captured using the two-dimensional NFEA. Compared with the B-C model, the present model based on the flexible interface theory predicts more accurate shear stresses for the long unbalanced SLJ. Except for two free ends, the shear stresses of adhesive interface determined by the present model correlate extremely well with the results predicted by NFEA. The small differences between the results of present model and the NFEA are induced to treat linearly the nonlinear terms in Eq. (18) and neglect the nonlinear terms in Eqs. (10) and (13). Similarly, from the Figs. 12b, d, 13b, d and 14b, d, it can be noted that the peel stresses of adhesive interface predicted by the present model agree well with the results determined by the NFEA. Due to neglecting the effect of geometrically nonlinearity for overlap region and interfacial compliance, the B-C model predicts the peel stresses of the adhesive interface with large deviations. Therefore, for adhesive stress analysis of the unbalanced SLJ, the effects of the interfacial compliance and the large deflection for the overlap and the adherends cannot be neglected.

Generally speaking, the geometrically nonlinear model based on flexible interface theory is validated through comparing with Cheng's model, B-C model and the NFEA. It is indicated vividly that the present one-dimensional beam model can predicate accurately the edge moment factors, transverse deflections and interfacial stresses for the unbalanced SLJ.

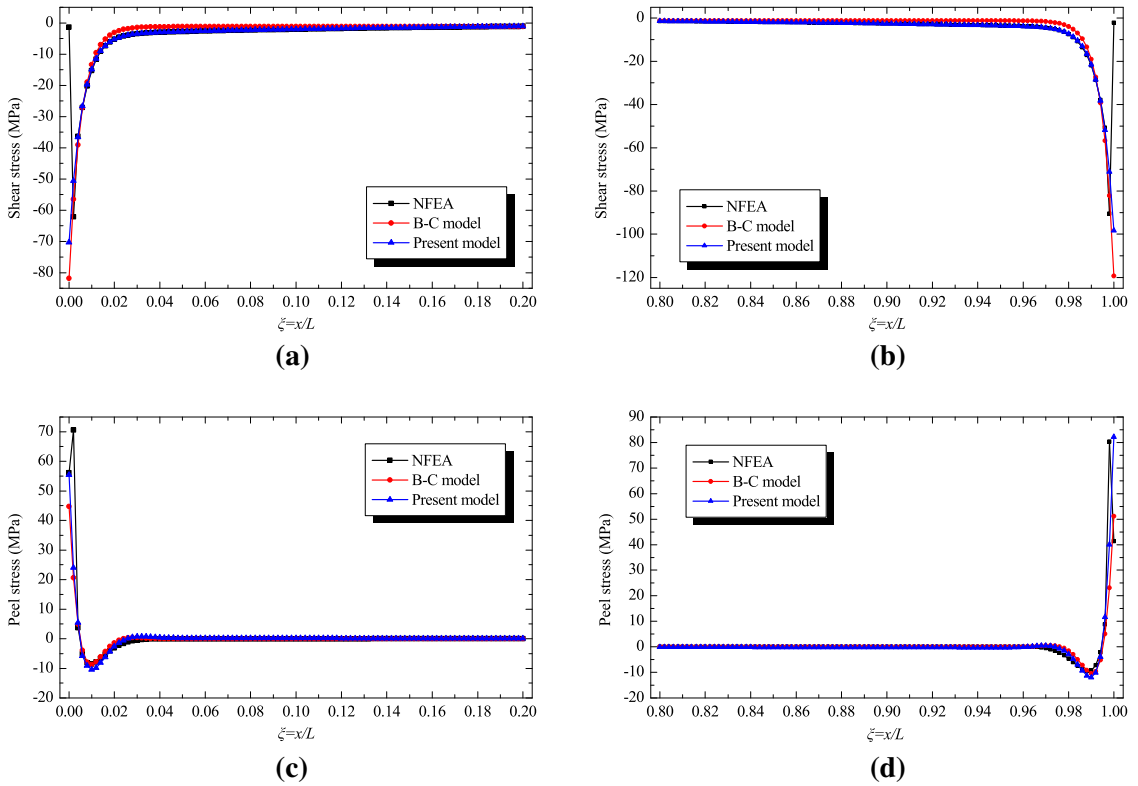

Fig. 14 Interfacial stresses for unbalanced SLJ with $L = 220$ under case 3: **a** shear stress along $0 \leq \xi \leq 0.2$; **b** peel stress along $0 \leq \xi \leq 0.2$; **c** shear stress along $0.8 \leq \xi \leq 1.0$; **d** peel stress along $0.8 \leq \xi \leq 1.0$

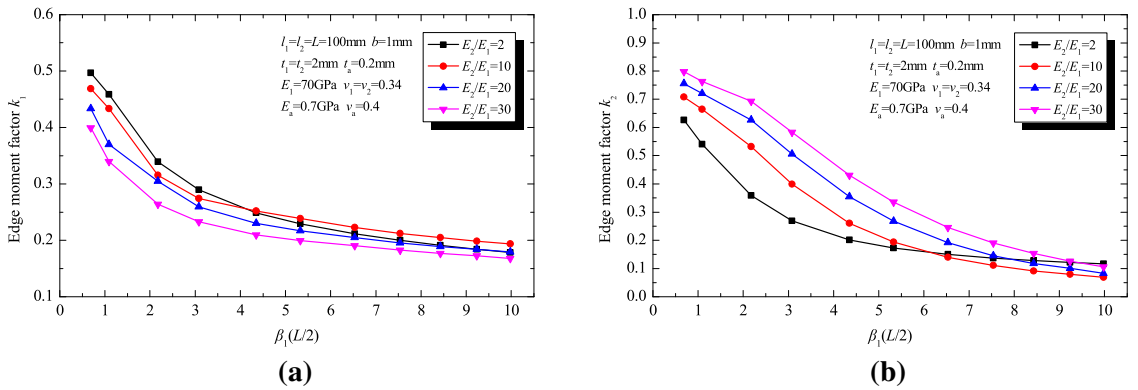

Fig. 15 Edge moment factors for unbalanced SLJ vary with different E_2/E_1: **a** edge moment factor k_1; **b** edge moment factor k_2

4 Parametric study

For the unbalanced SLJ under tensile loading, it is vital whether the edge moment factors are determined with high accuracy. Therefore, in order to further understand the edge moment factors for the unbalanced SLJ, the parametric studies concerning Young's modulus ratio and thickness ratio are performed using the present model in this section.

4.1 Effect of Young's modulus ratio E_2/E_1

The edge moment factors for the unbalanced SLJ with different E_2/E_1 are shown in Fig. 15. From the Fig. 15a, it can be noted that the edge moment factor k_1 decreases gradually as the Young's modulus ratio

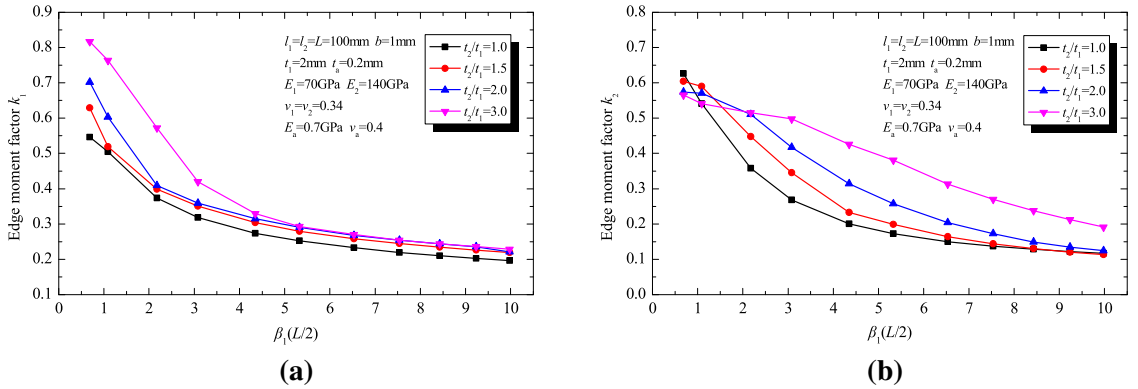

Fig. 16 Edge moment factors for unbalanced SLJ vary with different t_2/t_1: **a** edge moment factor k_1; **b** edge moment factor k_2

E_2/E_1 increases when $\beta_1(L/2) < 4$. While $\beta_1(L/2)$ approaches 10, the edge moment factor k_1 increases firstly and then decreases as the E_2/E_1 increases. Similarly, from Fig. 15b it is obtained that the edge moment factor k_2 increases gradually as E_2/E_1 increases when $\beta_1(L/2) < 6$. As $\beta_1(L/2)$ approaches 10, the edge moment factor k_2 decreases firstly and then increases when the E_2/E_1 increases.

4.2 Effect of thickness ratio t_2/t_1

From Fig. 16a, it can be obtained that the edge moment factor k_1 for the unbalanced SLJ increases as the thickness ratio t_2/t_1 increases gradually. Compared with the condition of $\beta_1(L/2) < 4$, the increase in amplifications of k_1 diminish when $\beta_1(L/2) \geq 4$, especially t_2/t_1 from 2 to 3. From Fig. 16b, it can be noted that the edge moment factor k_2 increases gradually as t_2/t_1 increases when $3 \leq \beta_1(L/2) \leq 7.5$. In contrast, when $\beta_1(L/2)$ approaches 0.7, the edge moment factor k_2 decreases gradually when the E_2/E_1 increases.

5 Conclusions

In this paper, the one-dimensional beam model considering simultaneously the effects of interface compliance and large deflection for the overlap and the adherends is presented. The edge moment factors, transverse deflections and interfacial stress distributions for the unbalanced SLJ under static tensile loading are predicted with the present solutions. Meanwhile, the applicability and accuracy of the present model are validated through comparing with the Cheng's model, B-C model and the results of NFEA. Finally, the effects of Young's modulus ratio and thickness ratio on the edge moment factors are studied using the present model. Some main conclusions are drawn, as follows:

(1) The governing equations based on the displacement compatibility condition of the flexible interface theory can capture the main features of geometrical nonlinearity for the unbalanced SLJ under static tensile loading.
(2) The present model can predict accurately the edge moment factors, transverse deflections and interfacial stresses for the unbalanced SLJ, whatever the unbalanced SLJ is composed of flexible, semiflexible or inflexible adhesive layer.
(3) As E_2/E_1 increases, the edge moment factor k_1 decreases when $\beta_1(L/2) < 4$ and the edge moment factor k_2 increases gradually when $\beta_1(L/2) < 6$; as t_2/t_1 increases, the edge moment factor k_1 increases accordingly and the edge moment factor k_2 increases gradually when $3 \leq \beta_1(L/2) \leq 7.5$.
(4) To further understand the nonlinear behavior of the unbalanced SLJ under static tensile loading, the theoretical studies considering the effects of the geometrically nonlinearity and material nonlinearity should be performed in the future.

Acknowledgments This research is sponsored by the Major State Basic Research Development Program of China (973 Program) (No.2012CB026200), the Fundamental Research Funds for the Central Universities (No.CXZZ13_0110), the Fundamental Research Funds for outstanding Doctoral Dissertation of Southeast university (No.YBJJ-1422).

References

1. Tsai, M.Y., Morton, J.: An evaluation of analytical and numerical-solutions to the single-lap joint. Int. J. Solids Struct. **31**(18), 2537–2563 (1994)
2. Yang, S., Xu, W., Liang, L.H., Wang, T.C., Wei, Y.G.: An experimental study on the dependence of the strength of adhesively bonded joints with thickness and mechanical properties of the adhesives. J. Adhes. Sci. Technol. **28**(11), 1055–1071 (2014)
3. Tong, L., Steven, G.P.: Analysis and Design of Structural Bonded Joints. Kluwer Academic Publishers, Boston (1999)
4. Zou, G.P., Shahin, K., Taheri, F.: An analytical solution for the analysis of symmetric composite adhesively bonded joints. Compos. Struct. **65**(3–4), 499–510 (2004)
5. Luo, Q., Tong, L.: Analytical solutions for adhesive composite joints considering large deflection and transverse shear deformation in adherends. Int. J. Solids Struct. **45**(22–23), 5914–5935 (2008)
6. Shahin, K., Kember, G., Taheri, F.: An asymptotic solution for evaluation of stresses in balanced and unbalanced adhesively bonded joints. Mech. Adv. Mater. Struct. **15**, 88–103 (2008)
7. Zhao, B., Lu, Z., Lu, Y.: Closed-form solutions for elastic stress–strain analysis in unbalanced adhesive single-lap joints considering adherend deformations and bond thickness. Int. J. Adhes. Adhes. **31**(6), 434–445 (2011)
8. Zhao, B., Lu, Z., Lu, Y.: Two-dimensional analytical solution of elastic stresses for balanced single-lap joints—variational method. Int. J. Adhes. Adhes. **49**, 115–126 (2014)
9. Tsai, M.Y., Morton, J., Krieger, R.B., Oplinger, D.W.: Experimental investigation of the thick-adherend lap shear test. J. Adv. Mater. **27**(3), 28–36 (1996)
10. Sawa, T., Liu, J., Nakano, K., Tanaka, J.: A two-dimensional stress analysis of single-lap adhesive joints of dissimilar adherends subjected to tensile loads. J. Adhes. Sci. Technol. **14**(1), 43–66 (2000)
11. Li, G., Lee-Sullivan, P.: Finite element and experimental studies on single-lap adhesive joints of dissimilar adherends subjected to tensile loads. Int. J. Adhes. Adhes. **21**(3), 211–220 (2001)
12. Kumar, R., Bhat, M.R., Murthy, C.: Experimental analysis of composite single-lap joints using digital image correlation and comparison with theoretical models. J. Reinf. Plast. Compos. **32**(23), 1858–1876 (2013)
13. Silva, T.C., Nunes, L.: A new experimental approach for the estimation of bending moments in adhesively bonded single lap joints. Int. J. Adhes. Adhes. **54**, 13–20 (2014)
14. Gultekin, K., Akpinar, S., Ozel, A.: The effect of the adherend width on the strength of adhesively bonded single-lap joint: Experimental and numerical analysis. Compos. Part B Eng. **60**, 736–745 (2014)
15. Pinto, A., Campilho, R., Mendes, I.R., Baptista, A.: Numerical and experimental analysis of balanced and unbalanced adhesive single-lap joints between aluminium adherends. J. Adhes. **90**(1SI), 89–103 (2014)
16. Hell, S., Weissgraeber, P., Felger, J., Becker, W.: A coupled stress and energy criterion for the assessment of crack initiation in single lap joints: a numerical approach. Eng. Fract. Mech. **117**, 112–126 (2014)
17. Goncalves, D., Campilho, R., Da Silva, L., Fernandes, J.: The use of the boundary element method in the analysis of single lap joints. J. Adhes. **90**(1SI), 50–64 (2014)
18. Oz, O., Ozer, H.: On the von Mises elastic stress evaluations in the bi-adhesive single-lap joint: a numerical and analytical study. J. Adhes. Sci. Technol. **28**(21), 2133–2153 (2014)
19. Ozer, H., Oz, O.: A comparative evaluation of numerical and analytical solutions to the biadhesive single-lap joint. Math. Probl. Eng. 852872 (2014). doi:10.1155/2014/852872
20. Luo, Q., Tong, L.: Fully-coupled nonlinear analysis of single lap adhesive joints. Int. J. Solids Struct. **44**(7–8), 2349–2370 (2007)
21. da Silva, L.F.M., Ochsner, A., Adams, R.D.: Handbook of Adhesion Technology. Springer, Berlin (2011)
22. da Silva, L.F.M., das Neves, P.J.C., Adams, R.D., et al.: Analytical models of adhesively bonded joints—Part I: Literature survey. Int. J. Adhes. Adhes. **29**, 319–330 (2009)
23. da Silva, L.F.M., das Neves, P.J.C., Adams, R.D., et al.: Analytical models of adhesively bonded joints—Part II: Comparative study. Int. J. Adhes. Adhes. **29**, 331–341 (2009)
24. Goland, M., Reissner, E.: The stresses in cemented joints. J. Appl. Mech. **11**, A17–A27 (1944)
25. Oplinger, D.W.: Effects of adherend deflections in single lap joints. Int. J. Solids Struct. **31**(18), 2565–2587 (1994)
26. Luo, Q., Tong, L.: Analytical solutions for nonlinear analysis of composite single-lap adhesive joints. Int. J. Adhes. Adhes. **29**(2), 144–154 (2009)
27. Srinivas, S.: Analysis of Bonded Joint. NASA TN D-7855.1975
28. Bigwood, D.A., Crocombe, A.D.: Elastic analysis and engineering design formula for bonded joints. Int. J. Adhes. Adhes. **9**(4), 229–242 (1989)
29. Adams, R.D., Mallick, V.: A method for the stress analysis of lap joints. J. Adhes. **38**(3–4), 199–217 (1992)
30. Cheng, S., Chen, D., Shi, Y.: analysis of adhesive-bonded joints with nonidentical adherends. J. Eng. Mech. **117**(3), 605–623 (1991)
31. Yang, C., Pang, S.S.: Stress–strain analysis of single-lap composite joints under tension. J. Eng. Mater. Technol. **118**(2), 247–255 (1996)
32. Li, G.: Deformation of Balanced and Unbalanced Adhesively Bonded Single-Lap Joints. The University of New Brunswick, Fredericton (2000)
33. Taheri, F., Zou, G.P.: Treatment of unsymmetric adhesively bonded composite sandwich panels-to-flange joints. Mech. Adv. Mater. Struct. **11**(2), 175–196 (2004)
34. Lee, J., Kim, H.: Stress analysis of generally asymmetric single lap joints adhesively bonded joints. J. Adhes. **81**(5), 443–472 (2005)
35. Qiao, P.Z., Chen, F.L.: An improved adhesively bonded bi-material beam model for plated beams. Eng. Struct. **30**(7), 1949–1957 (2008)
36. Chen, F.L., Qiao, P.Z.: On the intralaminar and interlaminar stress analysis of adhesive joints in plated beams. Int. J. Adhes. Adhes. **36**, 44–55 (2012)

37. Tsai, M.Y., Oplinger, D.W., Morton, J.: Improved theoretical solutions for adhesive lap joints. Int. J. Solids Struct. **35**(12), 1163–1185 (1998)
38. Carpenter, W.C.: Stresses in bonded connections using finite elements. Int. J. Numer. Methods Eng. **15**(11), 1659–1680 (1980)